Penalized Regression Methods for Interaction and Mixed-Effects Models with Applications to Genomic and Brain Imaging Data

Sahir Rai Bhatnagar

Doctor of Philosophy

Department of Epidemiology, Biostatistics and Occupational Health

McGill University
Montréal, Québec, Canada
July 2018

Dedication

This thesis is dedicated to my family, Dadi, Papa, Maa, Sameer, Marie-Pierre, Louis, Mathieu, Chandni, Amir, Navdeep, Carlos, Gloria, and Karen.

Acknowledgements

I am most grateful to Celia Greenwood and Yi Yang for the supervision of this thesis, their advice and guidance not only in professional issues, but also in all other fundamental aspects.

Preface & Contribution of Authors

Manuscript 1: Bhatnagar SR, Yang Y, Khundrakpam B, Evans A, Blanchette M, Bouchard L, Greenwood CMT (2017). An analytic approach for interpretable predictive models in high dimensional data, in the presence of interactions with exposures. Genetic Epidemiology. Apr 1;42(3):233-49. DOI 10.1002/gepi.22112.

Software: https://cran.r-project.org/package=eclust

SRB, CMTG, YY, and MB contributed to the conceptualization of this research; SRB, LB, and BK contributed to the data curation; SRB contributed to the formal analysis, software, visualization; SRB and CMTG contributed to the methodology; SRB and CMTG contributed to writing the original draft; All authors contributed to editing the draft.

Manuscript 2: Bhatnagar SR, Yang Y, Lovato A, Greenwood CMT (2018+). Sparse Additive Interaction Models.

Software: https://github.com/sahirbhatnagar/sail

Manuscript 3: Bhatnagar SR, Oualkacha K, Yang Y, Forest M, Greenwood CMT (2018+). A General Framework for Variable Selection in Linear Mixed Models with Applications to Genetic Studies with Structured Populations.

Software: https://github.com/sahirbhatnagar/ggmix

Abstract

In high-dimensional (HD) data, where the number of covariates (p) greatly exceeds the number of observations (n), estimation can benefit from the bet-on-sparsity principle, i.e., only a small number of predictors are relevant in the response. This assumption can lead to more interpretable models, improved predictive accuracy, and algorithms that are computationally efficient. In genomic and brain imaging studies, where the sample sizes are particularly small due to high data collection costs, we must often assume a sparse model because there isn't enough information to estimate p parameters. For these reasons, penalized regression methods such as the lasso and group-lasso have generated substantial interest since they can set model coefficients exactly to zero. In the penalized regression framework, many approaches have been developed for main effects. However, there is a need for developing interaction and mixed-effects models. Indeed, accurate capture of interactions may hold the potential to better understand biological phenomena and improve prediction accuracy since they may reflect important modulation of a biological system by an external factor. Furthermore, penalized mixed-effects models that account for correlations due to groupings of observations can improve sensitivity and specificity. This thesis is composed primarily of three manuscripts. The first manuscript describes a novel strategy called `eclust` for dimension reduction that leverages the effects of an exposure variable with broad impact on HD measures. With `eclust`, we found improved prediction and variable selection performance compared to methods that do not consider the exposure in the clustering step, or to methods that use the original data as features. We further illustrate this modeling framework through the analysis of three data sets from very different fields, each with HD data, a binary exposure, and a phenotype of interest. In the second manuscript, we propose a method called `sail` for detecting non-linear interactions that automatically enforces the strong heredity property using both the ℓ_1 and ℓ_2 penalty functions. We describe a blockwise coordinate descent procedure for solving the objective function and provide performance metrics on both simulated and real data. The third manuscript develops a general penalized mixed model

framework to account for correlations in genetic data due to relatedness called `ggmix`. Our method can accommodate several sparsity-inducing penalties such as the lasso, elastic net and group lasso and also readily handles prior annotation information in the form of weights. Our algorithm has theoretical guarantees of convergence and we again assess its performance in both simulated and real data. We provide efficient implementations of all our algorithms in open source software.

Abrégé

Il est aujourd'hui possible

Table of contents

List of Tables

List of Figures and Tables

Chapter 1

Introduction

In this thesis, we consider the prediction of an outcome variable y observed on n individuals from p variables, where p is much larger than n. Challenges in this high-dimensional (HD) context include not only building a good predictor which will perform well in an independent dataset, but also being able to interpret the factors that contribute to the predictions. This latter issue can be very challenging in ultra-high dimensional predictor sets. For example, multiple different sets of covariates may provide equivalent measures of goodness of fit (Fan et al., 2014), and therefore how does one decide which are important?

When $p >> n$, standard generalized linear models (GLMs) methodology cannot uniquely estimate the unknown coefficient vector β. Moreover, even when $p \leq n$ with p close to n, standard errors of GLMs are likely to be inflated and parameter estimates unstable (Reid et al., 2016). In these instances it may be useful to assume the *Bet on Sparsity Principle* which says:

> Use a procedure that does well in sparse problems, since no procedure does well
> in dense problems (J. Friedman et al., 2001).

In fact, sometimes this assumption is necessary since we often don't have a large enough sample size to estimate so many parameters. Even when we do, we might want to identify a

relatively small number of predictors that play an important role on the response. Applied researchers in the health sciences might prefer a simpler model because it can shed light on the etiology of disease. The sparsity assumption may also result in faster computations and more stable predictions on new datasets.

With the advent of high-throughput technologies in genomics and brain imaging studies, computational approaches to variable selection have become increasingly important. Broadly speaking, there are three main approaches to analyze such HD data: 1) univariate regression followed by a multiple testing correction 2) multivariable penalized regression and 3) dimension reduction followed by a multivariable regression.

In this thesis, we focus on the use of penalized regression methods for variable selection and prediction in HD settings. In Chapter 2, we provide a critical review of the literature on penalized regression methods and the computational algorithms used to fit these models. In Chapter 3, we develop the sparse additive interaction learning model `sail` for detecting non-linear interactions with a key environmental or exposure variable in HD data. In Chapter 4, we develop a general penalized linear mixed model framework called `ggmix` that simultaneously selects and estimates variables while accounting for between individual correlations in one step. Chapter 5 explores whether use of exposure-dependent clustering relationships in dimension reduction can improve predictive modelling in a two-step framework that we develop called `eclust`. Chapters 3, 4 and 5 were originally written as stand-alone papers and as a result, there is some inconsistency in notation. Chapter 5 has been published in *Genetic Epidemiology*. Chapters 3 and 4 will be submitted to a statistical journal shortly after the submission of the thesis. We have published open source and freely available `R` packages for each of the methods developed Chapters 3, 4 and 5 (available at https://github.com/sahirbhatnagar/). Table 1.1 provides an overview of our software packages including some of their key characteristics. In Chapter 6, we conclude with an overview of the three manuscripts.

Table 1.1: Overview of Our Software Packages

	eclust	sail	ggmix
Model			
Least-Squares	✓	✓	✓
Binary Classification	✓		
Survival Analysis			
Penalty			
Ridge	✓		✓
Lasso	✓	✓	✓
Elastic Net	✓		✓
Group Lasso		✓	✓
Feature			
Interactions	✓	✓	
Flexible Modeling	✓	✓	
Random Effects			✓
Data	(x, y, e)	(x, y, e)	$(x, y, \mathbf{\Psi})$

Chapter 2

Literature Review

The Literature Review is comprised of five sections. The first is a description of three general analytic strategies for high-dimensional data. The second and third sections describe two penalization methods that this thesis builds upon, namely the lasso and the group lasso. For each method we detail the algorithms used to fit these models and their convergence properties. In the fourth section we introduce penalized interaction models. This is followed by a brief introduction to linear mixed-effects models.

2.1 High-dimensional regression methods

We briefly introduce three of the main analytic strategies used to analyze HD data below.

2.1.1 Univariate regression

Genome-wide association studies (GWAS) have become the standard method for analyzing genetic datasets. A GWAS consists of a series of univariate regressions followed by a

multiple testing correction. This approach is simple and easy to implement, and has successfully identified thousands of genetic variants associated with complex diseases (https://www.genome.gov/gwastudies/). Despite these impressive findings, the discovered markers have only been able to explain a small proportion of the phenotypic variance known as the missing heritability problem (Manolio et al., 2009). One plausible explanation is that there are many causal variants that each explain a small amount of variation with small effect sizes (J. Yang et al., 2010). GWAS are likely to miss these true associations due to the stringent significance thresholds required to reduce the number of false positives (Manolio et al., 2009). Most statistical methods for performing multiple testing adjustments assume weak dependence among the variables being tested (Leek & Storey, 2008). Dependence among multiple tests can lead to incorrect Type 1 error rates (Lin et al., 2013) and highly variable significance measures (Leek & Storey, 2008). Even in the presence of weakly dependent variables, adjusting for multiple tests in whole genome studies can result in low power. Furthermore, the univariate regression approach does not allow for modeling the joint effect of many variants which may be biologically more plausible (Schadt, 2009). In the next section, we introduce multivariable penalized regression approaches which have been proposed to address some of these limitations.

2.1.2 Multivariable penalized regression

For n observations and p covariates, consider the multiple linear regression model $\boldsymbol{y} = \mathbf{X}\boldsymbol{\beta} + \boldsymbol{\varepsilon}$, where $\boldsymbol{y}$ is a n-length response vector, $\mathbf{X}$ is an $n \times p$ design matrix, $\boldsymbol{\beta}$ is a p-length coefficient vector and $\boldsymbol{\varepsilon}$ is a n-length error vector. The least squares estimate is given by $\widehat{\boldsymbol{\beta}} = \left(\mathbf{X}^T\mathbf{X}\right)^{-1}\mathbf{X}^T\boldsymbol{y}$. In high-dimensional data, the problem is that $\mathbf{X}^T\mathbf{X}$ is singular because the number of covariates greatly exceeds the number of subjects. For example DNA microarrays measure the expression of approximately 20,000 genes. However, due to funding constraints, the sample size is often less than a few hundred. A common solution to this

problem is through penalized regression, i.e., apply a constraint on the values of $\boldsymbol{\beta}$. The problem can be formulated as finding the vector $\boldsymbol{\beta}$ that minimizes the penalized sum of squares:

$$\underbrace{\sum_{i=1}^{n} \left(y_i - \beta_0 - \sum_{j=1}^{p} X_{ij} \beta_j \right)^2}_{\text{goodness of fit}} + \underbrace{\sum_{j=1}^{p} p(\beta_j; \lambda, \gamma)}_{\text{penalty}} \tag{2.1}$$

The first term of (2.1) is the squared loss of the data and can be generalized to any loss function while the second term is a penalty which depends on non-negative tuning parameters λ and γ that control the amount of shrinkage to be applied to $\boldsymbol{\beta}$ and the degree of concavity of the penalty function, respectively. Several penalty terms have been developed in the literature. Ridge regression places a bound on the square of the coefficients (ℓ_2 penalty) (Hoerl & Kennard, 1970) which has the effect of shrinking the magnitude of the coefficients. This however does not produce parsimonious models as none of the coefficients can be shrunk to exactly 0. The Lasso (Tibshirani, 1996) overcomes this problem by placing a bound on the sum of the absolute values of the coefficients (ℓ_1 penalty) which sets some of them to 0, thereby simultaneously performing model selection. The Lasso, along with other forms of penalization (e.g. SCAD Fan & Li (2001), Fused Lasso (Tibshirani et al., 2005), Adaptive Lasso (Zou, 2006), Relaxed Lasso (Meinshausen, 2007), MCP (C.-H. Zhang, 2010)) have proven successful in many practical problems. Despite these encouraging results, such methods have low sensitivity in the presence of high empirical correlations between covariates because only one variable tends to be selected from the group of correlated or nearly linearly dependent variables (Bühlmann et al., 2013). As a consequence, there is rarely consistency on which variable is chosen from one dataset to another (e.g. in cross-validation folds). This behavior may not be well suited to certain genomic datasets in which large sets of predictors are highly correlated (e.g. a regulatory module) and are also associated with the response. The elastic net was proposed to benefit from the strengths of ridge regression's treatment of correlated variables and lasso's sparsity (Zou & Hastie, 2005). By placing both an ℓ_1 and ℓ_2 penalty on $\boldsymbol{\beta}$, the elastic net achieves model parsimony while yielding similar re-

gression coefficients for correlated variables. These methods however do not take advantage of the grouping structure of the data. For example, cortical thickness measurements from magnetic resonance imaging (MRI) scans are often grouped into cortical regions of the Automated Anatomical Labelling (AAL) atlas (Tzourio-Mazoyer et al., 2002). Genes involved in the same cellular process (e.g. KEGG pathway (Kanehisa et al., 2008)) can also be placed into biologically meaningful groups. When regularizing with the ℓ_1 penalty, each variable is selected individually regardless of its position in the design matrix. Existing structures between the variables (e.g. spatial, networks, pathways) are ignored even though in many real-life applications the estimation can benefit from this prior knowledge in terms of both prediction accuracy and interpretability (Bach et al., 2012). The group lasso (Yuan & Lin, 2006) (and generalizations thereof) overcomes this problem by producing a structured sparsity (Bach et al., 2012), i.e., given a predetermined grouping of non-overlapping variables, all members of the group are either zero or non-zero. The main drawback when applying these methods to genomic data is that these groups may not be known *a priori*. Known pathways may not be relevant to the response of interest and the study of inferring gene networks is still in its infancy.

2.1.3   Dimension reduction together with regression

Due to the unknown grouping problem, several authors have suggested a two-step procedure where they first cluster or group variables in the design matrix and then subsequently proceed to model fitting where the feature space is some summary measure of each group. This idea dates back to 1957 when Kendall (Kendall, 1957) first proposed using principal components in regression. Hierarchical clustering based on the correlation of the design matrix has also been used to create groups of genes in microarray studies and for each level of hierarchy, the cluster average was used as the new set of potential predictors in forward-backward selection (Hastie et al., 2001) or the lasso (Park et al., 2007). Bühlmann et al. (2013) proposed a bottom-up

agglomerative clustering algorithm based on canonical correlations and used the group lasso on the derived clusters. There are some advantages to these methods over the ones previously mentioned in Sections 2.1.1 and 2.1.2. First, the results may be more interpretable than the traditional lasso (and related methods) because the non-zero components of the prediction model represent sets of genes as opposed to individual ones. Second, by using genes which cluster well, we bias the inputs towards correlated sets of genes which are more likely to have similar function. Third, taking a summary measure of the resulting clusters can reduce the variance in prediction (overfitting) due to the compressed dimension of the feature space. Lastly, from a practical point of view this approach is flexible and easy to implement because efficient algorithms exist for both clustering (Müllner, 2013) and model fitting (J. Friedman et al., 2010; Y. Yang & Zou, 2014).

In this context, we introduce a new two-step procedure called `eclust` (Bhatnagar et al., 2018) in Chapter 5 of the thesis. Our method is motivated by the fact that exposure variables (e.g. smoking) can alter correlation patterns between clusters of high-dimensional variables, i.e., alter network properties of the variables. However, it is not well understood whether such altered clustering is informative in prediction. In this paper, we explore whether use of exposure-dependent clustering relationships in dimension reduction can improve predictive modelling in a two-step framework.

A limitation of two-step methods is that the clustering is done in an unsupervised manner, i.e., the clusters do not use the response information. This has the effect of assigning similar coefficient values to correlated features. Witten et al. (2014) proposed a method which encourages features that share an association with the response to take on similar coefficient values. This is useful in situations where only a fraction of the features in a cluster are associated with the response.

2.2 Lasso

Consider the multiple linear regression model $\boldsymbol{y} = \beta_0 + \mathbf{X}\boldsymbol{\beta} + \boldsymbol{\varepsilon}$, where $\boldsymbol{y} \in \mathbb{R}^n$ is the response, $\mathbf{X} \in \mathbb{R}^{n \times p}$ is the design matrix, $\beta_0 \in \mathbb{R}$ is the intercept, $\boldsymbol{\beta} \in \mathbb{R}^p$ is the coefficient vector corresponding to $\mathbf{X}$ and $\boldsymbol{\varepsilon} \in \mathbb{R}^n$ is a vector of iid random errors. For least-squares loss, the lasso estimator (Tibshirani, 1996; Zou, 2006) is defined as

$$\widehat{\boldsymbol{\beta}}(\lambda) = \arg\min_{(\beta_0, \boldsymbol{\beta})} \frac{1}{2} \sum_{i=1}^{n} w_i (y_i - \beta_0 - (\mathbf{X}\boldsymbol{\beta})_i)^2 + \lambda \sum_{j=1}^{p} v_j |\beta_j| \tag{2.2}$$

where $(\mathbf{X}\boldsymbol{\beta})_i$ is the ith element of the n-length vector $\mathbf{X}\boldsymbol{\beta}$, $\lambda > 0$ is a tuning parameter which controls the amount of regularization, w_i is a known weight for the ith observation, and v_j is the penalty factor for the jth covariate. These penalty factors are known and allow parameters to be penalized differently. In particular, when $v_j = 1$ for $j = 1, \ldots, p$ then all parameters are regularized equally by λ, and when $v_j = 0$ the jth covariate is not penalized, i.e., it will always be included in the model. Note also that the intercept is not penalized. The estimator (2.2) simultaneously does variable selection and shrinks the regression coefficients towards 0. Depending on the choice of λ, $\widehat{\beta}_j(\lambda) = 0$ for some j's, and $\widehat{\beta}_j(\lambda)$ can be thought of as a shrunken least squares estimator (Bühlmann & Van De Geer, 2011). It is worth noting that (2.2) is a convex optimization problem and thus can be solved very efficiently using a block coordinate descent algorithm (J. Friedman et al., 2007; Tseng & Yun, 2009) for which we provide further details below. Other algorithms for solving this problem exist including LARS (Efron et al., 2004) and the homotopy algorithm (Osborne et al., 2000), but these have been largely preceded by the coordinate descent algorithm due to its speed and computational efficiency.

2.2.1 Block coordinate descent algorithm

In a series of seminal papers, Tseng lays the groundwork for a general purpose block coordinate descent algorithm (CGD) (Tseng, 2001; Tseng et al., 1988; Tseng & Yun, 2009) to minimize the sum of a smooth function f (i.e. continuously differentiable) and a separable convex function P of the form

$$Q_\lambda(\boldsymbol{\Theta}) = \arg\min_{\boldsymbol{\Theta}} \ f(\boldsymbol{\Theta}) + \lambda P(\boldsymbol{\Theta}) \tag{2.3}$$

At each iteration, the algorithm approximates $f(\boldsymbol{\Theta})$ in (2.3) by a strictly convex quadratic function and then applies block coordinate decent to generate a decent direction followed by an inexact line search along this direction (Tseng & Yun, 2009). For continuously differentiable $f(\cdot)$ and convex and block-separable $P(\cdot)$ (e.g. $P(\boldsymbol{\beta}) = \sum_i P_i(\beta_i)$), Tseng & Yun (2009) show that the solution generated by the CGD method is a stationary point of (2.3) if the coordinates are updated in a Gauss-Seidel manner, i.e., $Q_\lambda(\boldsymbol{\Theta})$ is minimized with respect to one parameter while holding all others fixed. The separability of the penalty function into a sum of functions of each individual parameter is the key to applying this algorithm to lasso type problems. Indeed, the CGD algorithm has been successfully applied in fixed effects models (J. Friedman et al., 2010; Meier et al., 2008) and linear mixed models (Schelldorfer et al., 2011). Following Tseng & Yun (2009), the general purpose CGD algorithm for solving (2.3) is given by Algorithm 1.

Algorithm 1: Coordinate Gradient Descent Algorithm to solve (2.3)

Set the iteration counter $k \leftarrow 0$ and choose initial values for the parameter vector $\boldsymbol{\Theta}^{(0)}$;

repeat

    Approximate the Hessian $\nabla^2 f(\boldsymbol{\Theta}^{(k)})$ by a symmetric matix $H^{(k)}$:

$$H^{(k)} = \text{diag}\left[\min\left\{\max\left\{\left[\nabla^2 f(\boldsymbol{\Theta}^{(k)})\right]_{jj}, 10^{-2}\right\} 10^9\right\}\right]_{j=1,\ldots,p} \qquad (2.4)$$

    for $j = 1, \ldots, p$ **do**

        Solve the descent direction $d^{(k)} := d_{H^{(k)}}(\Theta_j^{(k)})$;

$$d_{H^{(k)}}(\Theta_j^{(k)}) \leftarrow \arg\min_d \left\{\nabla f(\Theta_j^{(k)})d + \frac{1}{2}d^2 H_{jj}^{(k)} + \lambda P(\Theta_j^{(k)} + d)\right\} \qquad (2.5)$$

        Choose a stepsize;

$$\alpha_j^{(k)} \leftarrow \text{line search given by the Armijo rule}$$

        Update;

$$\widehat{\Theta}_j^{(k+1)} \leftarrow \widehat{\Theta}_j^{(k)} + \alpha_j^{(k)} d^{(k)}$$

    end

    $k \leftarrow k + 1$

until *convergence criterion is satisfied*;

The Armijo rule is defined as follows (Tseng & Yun, 2009):

Choose $\alpha_{init}^{(k)} > 0$ and let $\alpha^{(k)}$ be the largest element of $\left\{\alpha_{init}^{k}\delta^{r}\right\}_{r=0,1,2,\dots}$ satisfying

$$Q_\lambda(\Theta_j^{(k)} + \alpha^{(k)}d^{(k)}) \leq Q_\lambda(\Theta_j^{(k)}) + \alpha^{(k)}\varrho\Delta^{(k)} \tag{2.6}$$

where $0 < \delta < 1$, $0 < \varrho < 1$, $0 \leq \gamma < 1$ and

$$\Delta^{(k)} := \nabla f(\Theta_j^{(k)})d^{(k)} + \gamma(d^{(k)})^2 H_{jj}^{(k)} + \lambda P(\Theta_j^{(k)} + d^{(k)}) - \lambda P(\Theta_j^{(k)}) \tag{2.7}$$

Common choices for the constants are $\delta = 0.1$, $\varrho = 0.001$, $\gamma = 0$, $\alpha_{init}^{(k)} = 1$ for all k (Bertsekas, 1999). In what follows, we use Algorithm 1 to solve the lasso estimator with least-squares loss given by (2.2). Without loss of generality, we assume the penalty factors (v_j) are all equal to 1.

Descent Direction

For simplicity, we remove the iteration counter (k) from the derivation below.
For $\Theta_j^{(k)} \in \{\beta_1, \dots, \beta_p\}$, let

$$d_H(\Theta_j) = \arg\min_d G(d) \tag{2.8}$$

where

$$G(d) = \nabla f(\Theta_j)d + \frac{1}{2}d^2 H_{jj} + \lambda|\Theta_j + d|$$

Since $G(d)$ is not differentiable at $-\Theta_j$, we calculate the subdifferential $\partial G(d)$ and search for d with $0 \in \partial G(d)$:

$$\partial G(d) = \nabla f(\Theta_j) + dH_{jj} + \lambda u \tag{2.9}$$

where

$$
u = \begin{cases} 1 & \text{if} \quad d > -\Theta_j \\ -1 & \text{if} \quad d < -\Theta_j \\ [-1, 1] & \text{if} \quad d = \Theta_j \end{cases} \tag{2.10}
$$

We consider each of the three cases in (2.9) below

1. $d > -\Theta_j$

$$
\partial G(d) = \nabla f(\Theta_j) + dH_{jj} + \lambda = 0
$$
$$
d = \frac{-(\nabla f(\Theta_j) + \lambda)}{H_{jj}}
$$

Since $\lambda > 0$ and $H_{jj} > 0$, we have

$$
\frac{-(\nabla f(\Theta_j) - \lambda)}{H_{jj}} > \frac{-(\nabla f(\Theta_j) + \lambda)}{H_{jj}} = d \overset{\text{def}}{>} -\Theta_j
$$

The solution can be written compactly as

$$
d = \text{mid} \left\{ \frac{-(\nabla f(\Theta_j) - \lambda)}{H_{jj}}, -\Theta_j, \frac{-(\nabla f(\Theta_j) + \lambda)}{H_{jj}} \right\}
$$

where mid $\{a, b, c\}$ denotes the median (mid-point) of a, b, c.

2. $d < -\Theta_j$

$$
\partial G(d) = \nabla f(\Theta_j) + dH_{jj} - \lambda = 0
$$
$$
d = \frac{-(\nabla f(\Theta_j) - \lambda)}{H_{jj}}
$$

Since $\lambda > 0$ and $H_{jj} > 0$, we have

$$
\frac{-(\nabla f(\Theta_j) + \lambda)}{H_{jj}} < \frac{-(\nabla f(\Theta_j) - \lambda)}{H_{jj}} = d \overset{\text{def}}{<} -\Theta_j
$$

Again, the solution can be written compactly as

$$d = \text{mid} \left\{ \frac{-(\nabla f(\Theta_j) - \lambda)}{H_{jj}}, -\Theta_j, \frac{-(\nabla f(\Theta_j) + \lambda)}{H_{jj}} \right\}$$

3. $d_j = -\Theta_j$

There exists $u \in [-1, 1]$ such that

$$\partial G(d) = \nabla f(\Theta_j) + dH_{jj} + \lambda u = 0$$
$$d = \frac{-(\nabla f(\Theta_j) + \lambda u)}{H_{jj}}$$

For $-1 \le u \le 1$, $\lambda > 0$ and $H_{jj} > 0$ we have

$$\frac{-(\nabla f(\Theta_j) + \lambda)}{H_{jj}} \le d \overset{\text{def}}{=} -\Theta_j \le \frac{-(\nabla f(\Theta_j) - \lambda)}{H_{jj}}$$

The solution can again be written compactly as

$$d = \text{mid} \left\{ \frac{-(\nabla f(\Theta_j) - \lambda)}{H_{jj}}, -\Theta_j, \frac{-(\nabla f(\Theta_j) + \lambda)}{H_{jj}} \right\}$$

We see all three cases lead to the same solution for (2.8). Therefore the descent direction for $\Theta_j^{(k)} \in \{\beta_1, \ldots, \beta_p\}$ for the ℓ_1 penalty is given by

$$d = \text{mid} \left\{ \frac{-(\nabla f(\beta_j) - \lambda)}{H_{jj}}, -\beta_j, \frac{-(\nabla f(\beta_j) + \lambda)}{H_{jj}} \right\} \tag{2.11}$$

Solution for the β parameter

If the Hessian $\nabla^2 f(\mathbf{\Theta}^{(k)}) > 0$ then $H^{(k)}$ defined in (2.4) is equal to $\nabla^2 f(\mathbf{\Theta}^{(k)})$. Using $\alpha_{init} = 1$, the largest element of $\left\{ \alpha_{init}^{(k)} \delta^r \right\}_{r=0,1,2,\ldots}$ satisfying the Armijo Rule inequality is reached for $\alpha^{(k)} = \alpha_{init}^{(k)} \delta^0 = 1$. The Armijo rule update for the $\boldsymbol{\beta}$ parameter is then given

by

$$\beta_j^{(k+1)} \leftarrow \beta_j^{(k)} + d^{(k)}, \qquad j = 1, \ldots, p \tag{2.12}$$

Substituting the descent direction given by (2.11) into (2.12) we get

$$\beta_j^{(k+1)} = \text{mid} \left\{ \beta_j^{(k)} + \frac{-(\nabla f(\beta_j^{(k)}) - \lambda)}{H_{jj}}, 0, \beta_j^{(k)} + \frac{-(\nabla f(\beta_j^{(k)}) + \lambda)}{H_{jj}} \right\} \tag{2.13}$$

We can further simplify this expression. First, we can re-write the loss function in (2.2) as

$$g(\boldsymbol{\beta}^{(k)}) = \frac{1}{2} \sum_{i=1}^{n} w_i \left(y_i - \sum_{\ell \neq j} X_{i\ell} \beta_\ell^{(k)} - X_{ij} \beta_j^{(k)} \right)^2 \tag{2.14}$$

The gradient and Hessian are given by

$$\nabla f(\beta_j^{(k)}) \coloneqq \frac{\partial}{\partial \beta_j^{(k)}} g(\boldsymbol{\beta}^{(k)}) = - \sum_{i=1}^{n} w_i X_{ij} \left(y_i - \sum_{\ell \neq j} X_{i\ell} \beta_\ell^{(k)} - X_{ij} \beta_j^{(k)} \right) \tag{2.15}$$

$$H_{jj} \coloneqq \frac{\partial^2}{\partial \beta_j^{(k)2}} g(\boldsymbol{\beta}^{(k)}) = \sum_{i=1}^{n} w_i X_{ij}^2 \tag{2.16}$$

Substituting (2.15) and (2.16) into $\beta_j^{(k)} + \frac{-(\nabla f(\beta_j^{(k)}) - \lambda)}{H_{jj}}$

$$\beta_j^{(k)} + \frac{\sum_{i=1}^{n} w_i X_{ij} \left(y_i - \sum_{\ell \neq j} X_{i\ell} \beta_\ell^{(k)} - X_{ij} \beta_j^{(k)} \right) + \lambda}{\sum_{i=1}^{n} w_i X_{ij}^2}$$

$$= \beta_j^{(k)} + \frac{\sum_{i=1}^{n} w_i X_{ij} \left(y_i - \sum_{\ell \neq j} X_{i\ell} \beta_\ell^{(k)} \right) + \lambda}{\sum_{i=1}^{n} w_i X_{ij}^2} - \frac{\sum_{i=1}^{n} w_i X_{ij}^2 \beta_j^{(k)}}{\sum_{i=1}^{n} w_i X_{ij}^2}$$

$$= \frac{\sum_{i=1}^{n} w_i X_{ij} \left(y_i - \sum_{\ell \neq j} X_{i\ell} \beta_\ell^{(k)} \right) + \lambda}{\sum_{i=1}^{n} w_i X_{ij}^2} \tag{2.17}$$

Similarly, substituting (2.15) and (2.16) in $\beta_j^{(k)} + \frac{-(\nabla f(\beta_j^{(k)}) + \lambda)}{H_{jj}}$ we get

$$\frac{\sum_{i=1}^n w_i X_{ij} \left(y_i - \sum_{\ell \neq j} X_{i\ell} \beta_\ell^{(k)} \right) - \lambda}{\sum_{i=1}^n w_i X_{ij}^2} \tag{2.18}$$

Finally, substituting (2.17) and (2.18) into (2.13) we get

$$\beta_j^{(k+1)} = \text{mid} \left\{ \frac{\sum_{i=1}^n w_i X_{ij} \left(y_i - \sum_{\ell \neq j} X_{i\ell} \beta_\ell^{(k)} \right) - \lambda}{\sum_{i=1}^n w_i X_{ij}^2}, 0, \frac{\sum_{i=1}^n w_i X_{ij} \left(y_i - \sum_{\ell \neq j} X_{i\ell} \beta_\ell^{(k)} \right) + \lambda}{\sum_{i=1}^n w_i X_{ij}^2} \right\}$$

$$= \frac{\mathcal{S}_\lambda \left(\sum_{i=1}^n w_i X_{ij} \left(y_i - \sum_{\ell \neq j} X_{i\ell} \beta_\ell^{(k)} \right) \right)}{\sum_{i=1}^n w_i X_{ij}^2} \tag{2.19}$$

Where $\mathcal{S}_\lambda(x)$ is the soft-thresholding operator

$$\mathcal{S}_\lambda(x) = \text{sign}(x)(|x| - \lambda)_+$$

$\text{sign}(x)$ is the signum function

$$\text{sign}(x) = \begin{cases} -1 & x < 0 \\ 0 & x = 0 \\ 1 & x > 0 \end{cases}$$

and $(x)_+ = \max(x, 0)$. Since there is a closed form solution, which can be computed very quickly for each parameter update (given by (2.19)), the CGD algorithm is an attractive approach for solving the lasso estimator.

2.2.2   Lambda sequence

In general, the solution to (2.2) is computed over a decreasing sequence of values for the tuning parameter λ, beginning with the smallest value λ_{max} for which the entire coefficient vector $\widehat{\boldsymbol{\beta}} = \mathbf{0}_p$ (J. Friedman et al., 2010). To determine λ_{max}, we turn to the Karush-Kuhn-Tucker (KKT) optimality conditions for (2.2). These conditions can be written as

$$\frac{1}{v_j} \sum_{i=1}^{n} w_i X_{ij} \left(y_i - \sum_{j=1}^{p} X_{ij} \hat{\beta}_j \right) = \lambda \gamma_j,$$

$$\gamma_j \in \begin{cases} \text{sign}(\hat{\beta}_j) & \text{if} \quad \hat{\beta}_j \neq 0 \\ [-1, 1] & \text{if} \quad \hat{\beta}_j = 0 \end{cases}, \qquad \text{for } j = 1, \ldots, p \tag{2.20}$$

where γ_j is the subgradient of the function $f(x) = |x|$ evaluated at $x = \hat{\beta}_j$. From (2.20), we can solve for the smallest value of λ such that the entire vector $(\hat{\beta}_1, \ldots, \hat{\beta}_p)$ is 0. This is given by

$$\lambda_{max} = \max_{j} \left\{ \left| \frac{1}{v_j} \sum_{i=1}^{n} w_i X_{ij} y_i \right| \right\}, \quad j = 1, \ldots, p \tag{2.21}$$

Following J. Friedman et al. (2010), we can choose $\tau \lambda_{max}$ to be the smallest value of tuning parameters λ_{min}, and construct a sequence of K values decreasing from λ_{max} to λ_{min} on the log scale. The defaults are set to $K = 100$, $\tau = 0.01$ if $n < p$ and $\tau = 0.001$ if $n \geq p$. The optimal value of λ can be chosen using 5-fold or 10-fold cross-validation. For least-squares loss, this corresponds to choosing the λ which minimizes the mean squared error.

2.2.3   Warm starts

The way in which we have derived the sequence of tuning parameters using the KKT conditions, allows us to exploit warm starts which has been shown to lead to computational speedups (J. Friedman et al., 2010). That is, the solution $\widehat{\boldsymbol{\Theta}}$ for λ_k is used as the initial value $\boldsymbol{\Theta}^{(0)}$ for λ_{k+1}.

2.2.4 Adaptive lasso

It has been shown that the lasso estimator can be produce biased estimates for large coefficients and give inconsistent variable selection results at the optimal λ for prediction, i.e., many noise features are included in the prediction model (Zou, 2006). To overcome the bias problems of the lasso, Zou (2006) proposed the adaptive lasso which allows a different amount of shrinkage for each regression coefficient using adaptive weights. Adaptive weighting has been shown to construct oracle procedures (Fan & Li, 2001), i.e., asymptotically, it performs as well as if the true model were given in advance. The adaptive lasso can be described as a two-stage procedure:

1. Calculate the initial regression estimates $\widehat{\boldsymbol{\beta}}_{init}$ from (2.2)

2. Refit (2.2) using penalty factors v_j equal to $1/\left|\hat{\beta}_{init,j}\right|$ for $j = 1, \ldots, p$.

As we can see from the weights, the adaptive lasso will shrink larger coefficients less which leads to consistent variable selection results under weaker conditions than the lasso (Bühlmann & Van De Geer, 2011). We detail the adaptive lasso procedure in Algorithm 2.

Algorithm 2: Adaptive lasso algorithm

1. For a decreasing sequence $\lambda = \lambda_{max}, \ldots, \lambda_{min}$, fit the lasso with $v_j = 1$ for $j = 1, \ldots, p$
2. Use cross-validation or a data splitting procedure to determine the optimal value for the tuning parameter: $\lambda^{[opt]} \in \{\lambda_{max}, \ldots, \lambda_{min}\}$
3. Let $\hat{\beta}_{init,j}^{[opt]}$ for $j = 1, \ldots, p$ be the coefficient estimates corresponding to the model at $\lambda^{[opt]}$
4. Set the weights to be $v_j = \left(\left|\hat{\beta}_{init,j}^{[opt]}\right|\right)^{-1}$ for $j = 1, \ldots, p$
5. Refit the lasso with the weights defined in step 4), and use cross-validation or a data splitting procedure to choose the optimal value of λ

2.3 Group Lasso

One main drawback of the lasso is that it ignores the grouping structure of the design matrix. When given a predetermined grouping of non-overlapping variables, we would want
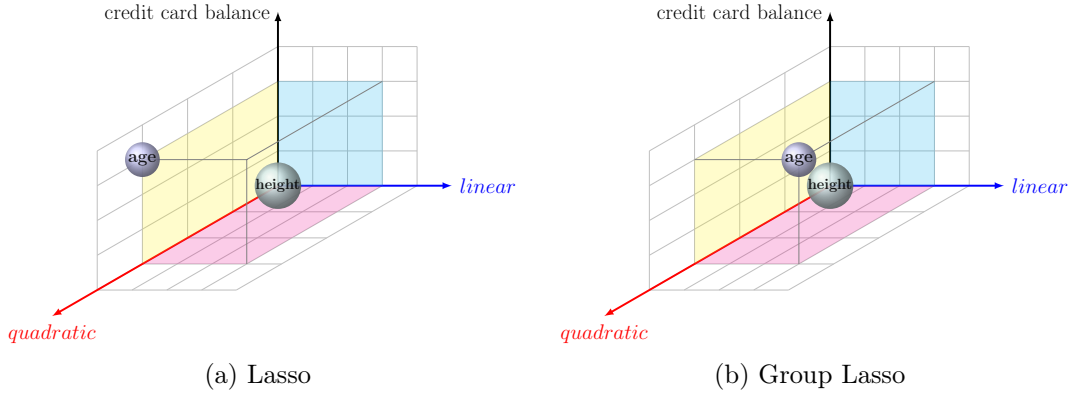
(a) Lasso (b) Group Lasso

Figure 2.1: The selected components from Model (2.22) for (a) the lasso and (b) the group lasso. In this toy example, the lasso selects only the quadratic term for age while the group lasso selects both linear and quadratic terms.

all members of the group to be either zero or non-zero. For example, when dealing with categorical predictors where each factor is expressed through a set of indicator variables, removing an irrelevant factor is equivalent to setting the coefficients of the indicator variables to 0. In an additive model, where each variable is projected on to a set of basis function, e.g. $f_j(X_j) = \sum_{\ell=1}^{m_j} \psi_{j\ell}(X_j)\beta_{j\ell}$, we would want all $\{\beta_{j\ell}\}_{\ell=1}^{m_j}$ to be either zero or non-zero. This key difference between the lasso and group lasso penalty is shown in Figure 2.1. Suppose we want to predict an individual's credit card balance from their age and height using the following additive model:

$$\text{credit card balance} = \beta_0 + \beta_{11}\text{age} + \beta_{12}\text{age}^2 + \beta_{21}\text{height} + \beta_{22}\text{height}^2 + \varepsilon \qquad (2.22)$$

In Figures 2.1a and 2.1b we see that both the lasso and group lasso set the linear and quadratic terms for height $(\hat{\beta}_{21}, \hat{\beta}_{22})$ to 0. However, the lasso estimates only a nonzero quadratic term for age $(\hat{\beta}_{11} = 0, \hat{\beta}_{12} \neq 0)$ while the group lasso estimates both linear and quadratic terms to be nonzero $(\hat{\beta}_{11} \neq 0, \hat{\beta}_{12} \neq 0)$. We now provide details on the group lasso estimator.

Assume that the predictors in the design matrix $\mathbf{X} \in \mathbb{R}^{n \times p}$ belong to K groups and define the

cardinality of index set I_k to be p_k. These groups are known *a priori* such that $(1, 2, \ldots, p) = \bigcup_{k=1}^{K} I_k$, and are also non-overlapping, i.e., $I_k \bigcap I_{k'} = \emptyset$ for $k \neq k'$. Therefore, group k contains p_k predictors corresponding to $\mathbf{X}^{(k)}$, i.e., the columns of the design matrix X_j for $j \in I_k$, and $1 \leq k \leq K$. The intercept belongs to its own group, i.e., $I_1 = \{1\}$. The group lasso partitions the variable coefficients into K groups $\boldsymbol{\beta} = ([\boldsymbol{\beta}^{(1)}]^{\mathsf{T}}, [\boldsymbol{\beta}^{(2)}]^{\mathsf{T}}, \cdots, [\boldsymbol{\beta}^{(K)}]^{\mathsf{T}})^{\mathsf{T}}$, where $\boldsymbol{\beta}^{(k)}$ denotes the segment of $\boldsymbol{\beta}$ corresponding to group k. For least-squares loss, the group lasso estimator (Yuan & Lin, 2006) is given by:

$$\widehat{\boldsymbol{\beta}}(\lambda) = \underset{(\beta_0, \boldsymbol{\beta})}{\arg\min} \frac{1}{2} \sum_{i=1}^{n} w_i (y_i - \beta_0 - (\mathbf{X}\boldsymbol{\beta})_i)^2 + \lambda \sum_{k=1}^{K} v_k \|\boldsymbol{\beta}^{(k)}\|_2 \tag{2.23}$$

where $\left\|\boldsymbol{\beta}^{(k)}\right\|_2 = \sqrt{\sum_{j \in I_k} \beta_j^2}$ and $\lambda > 0$ is the tuning parameter. As in the lasso estimator (2.2), there are both observation weights w_i, and penalty factors $v_k \geq 0$ which control the relative strength of the terms within the group lasso penalty. These penalty factors are often set to $\sqrt{p_k}$ (Yuan & Lin, 2006). Note that the same penalty factor is applied to all the coefficients in a group. Solving the group lasso estimator is more challenging than the lasso since there is no closed form solution for (2.23). In the next section, we detail a majorization-minimization (MM) type algorithm (Lange et al., 2000; Y. Yang & Zou, 2015) used to solve (2.23).

2.3.1 Groupwise majorization descent algorithm

This description of the groupwise majorization descent (GMD) algorithm used to solve (2.23) follows mainly from Y. Yang & Zou (2015). The main difference here is that we consider a more general loss function of the form

$$L(\boldsymbol{\beta} \mid \mathbf{D}) = \frac{1}{2} [\boldsymbol{y} - \widehat{\boldsymbol{y}}]^{\top} \mathbf{W} [\boldsymbol{y} - \widehat{\boldsymbol{y}}] \tag{2.24}$$

where $\widehat{\boldsymbol{y}} = \hat{\beta}_0 + \mathbf{X}\widehat{\boldsymbol{\beta}}$, $\mathbf{D}$ is the working data $\{\boldsymbol{y}, \mathbf{X}\}$, and $\mathbf{W}$ is an $n \times n$ nonsingular and known weight matrix. This weight matrix can be used when the elements of $\boldsymbol{y}$ are correlated as is done in generalized least squares. The original proposal in Y. Yang & Zou (2015) is a special case of (2.24) where $\mathbf{W}$ is a diagonal matrix with entries equal to w_i. The loss function (2.24) satisfies the quadratic majorization (QM) condition, since $L(\boldsymbol{\beta} \mid \mathbf{D})$ is differentiable as a function of $\boldsymbol{\beta}$, i.e., $\nabla L(\boldsymbol{\beta}|\mathbf{D}) = -(\boldsymbol{y} - \hat{\boldsymbol{y}})^\top \mathbf{W}\mathbf{X}$, and there exists a $p \times p$ matrix $\mathbf{H} = \mathbf{X}^\top \mathbf{W}\mathbf{X}$ which only depends on the data $\mathbf{D}$, such that for all $\boldsymbol{\beta}, \boldsymbol{\beta}^*$,

$$L(\boldsymbol{\beta} \mid \mathbf{D}) \leq L(\boldsymbol{\beta}^* \mid \mathbf{D}) + (\boldsymbol{\beta} - \boldsymbol{\beta}^*)^\top \nabla L(\boldsymbol{\beta}^*|\mathbf{D}) + \frac{1}{2}(\boldsymbol{\beta} - \boldsymbol{\beta}^*)^\top \mathbf{H}(\boldsymbol{\beta} - \boldsymbol{\beta}^*). \qquad (2.25)$$

We can exploit the fact that the loss function (2.24) satisfies the QM condition to majorize the loss function in (2.23) by (2.25), and that the penalty term $\sum_{k=1}^{K} v_k \|\boldsymbol{\beta}^{(k)}\|_2$ in (2.23) is separable with respect to the indices of the variables $k = 1, \ldots, K$ to performs groupwise updates for each $\boldsymbol{\beta}^{(k)}$.

Let $\widetilde{\boldsymbol{\beta}}$ denote the current solution of $\boldsymbol{\beta}$ and define $\mathbf{H}^{(k)}$ as the sub-matrix of $\mathbf{H}$ corresponding to group k. For example, if group 2 is $\{2, 4\}$ then $\mathbf{H}^{(2)}$ is a 2×2 matrix with

$$\mathbf{H}^{(2)} = \begin{bmatrix} h_{2,2} & h_{2,4} \\ h_{4,2} & h_{4,4} \end{bmatrix},$$

where $h_{i,j}$ is the i, jth entry of the $\mathbf{H}$ matrix. Write $\boldsymbol{\beta}$ such that $\boldsymbol{\beta}^{(k')} = \widetilde{\boldsymbol{\beta}}^{(k')}$ for $k' \neq k$. Given $\boldsymbol{\beta}^{(k')} = \widetilde{\boldsymbol{\beta}}^{(k')}$ for $k' \neq k$, the estimator for $\boldsymbol{\beta}^{(k)}$ is given by

$$\widehat{\boldsymbol{\beta}}^{(k)}(\lambda) = \arg\min_{\boldsymbol{\beta}^{(k)}} L(\boldsymbol{\beta} \mid \mathbf{D}) + \lambda v_k \|\boldsymbol{\beta}^{(k)}\|_2. \qquad (2.26)$$

Using $\boldsymbol{\beta} - \widetilde{\boldsymbol{\beta}} = (\underbrace{0, \ldots, 0}_{k-1}, \boldsymbol{\beta}^{(k)} - \widetilde{\boldsymbol{\beta}}^{(k)}, \underbrace{0, \ldots, 0}_{K-k})$ and the majorization defined in (2.25) we can

write

$$L(\boldsymbol{\beta} \mid \mathbf{D}) \leq L(\widetilde{\boldsymbol{\beta}} \mid \mathbf{D}) - (\boldsymbol{\beta}^{(k)} - \widetilde{\boldsymbol{\beta}}^{(k)})^{\top} U^{(k)} + \frac{1}{2}(\boldsymbol{\beta}^{(k)} - \widetilde{\boldsymbol{\beta}}^{(k)})^{\top} \mathbf{H}^{(k)}(\boldsymbol{\beta}^{(k)} - \widetilde{\boldsymbol{\beta}}^{(k)}). \quad (2.27)$$

where

$$U^{(k)} = \frac{\partial}{\partial \boldsymbol{\beta}^{(k)}} L(\boldsymbol{\beta} \mid \mathbf{D}) = -(\boldsymbol{y} - \hat{\boldsymbol{y}})^{\top} \mathbf{W} \mathbf{X}^{(k)}, \quad (2.28)$$

$$\mathbf{H}^{(k)} = \frac{\partial^2}{\partial \boldsymbol{\beta}^{(k)} \partial \boldsymbol{\beta}^{(k)\top}} L(\boldsymbol{\beta} \mid \mathbf{D}) = (\mathbf{X}^{(k)})^{\top} \mathbf{W} \mathbf{X}^{(k)}. \quad (2.29)$$

The upper bound in (2.27) can be majorized even further to avoid expensive matrix multiplications and storing $\mathbf{H}^{(k)}$ in memory. Let η_k be the largest eigenvalue of $\mathbf{H}^{(k)}$. We set $\gamma_k = (1 + \varepsilon^*)\eta_k$, where $\varepsilon^* = 10^{-6}$ and substitute γ_k for $\mathbf{H}^{(k)}$ in (2.27):

$$L(\boldsymbol{\beta} \mid \mathbf{D}) \leq L(\widetilde{\boldsymbol{\beta}} \mid \mathbf{D}) - (\boldsymbol{\beta}^{(k)} - \widetilde{\boldsymbol{\beta}}^{(k)})^{\top} U_{(k)} + \frac{1}{2}\gamma_k(\boldsymbol{\beta}^{(k)} - \widetilde{\boldsymbol{\beta}}^{(k)})^{\top}(\boldsymbol{\beta}^{(k)} - \widetilde{\boldsymbol{\beta}}^{(k)}). \quad (2.30)$$

It is important to note that the inequality strictly holds unless when $\boldsymbol{\beta}^{(k)} = \widetilde{\boldsymbol{\beta}}^{(k)}$. Substituting the upper bound in (2.30) for $L(\boldsymbol{\beta} \mid \mathbf{D})$ in (2.26) we get the following estimator for $\boldsymbol{\beta}^{(k)}$

$$\arg \min_{\boldsymbol{\beta}^{(k)}} L(\widetilde{\boldsymbol{\beta}} \mid \mathbf{D}) - (\boldsymbol{\beta}^{(k)} - \widetilde{\boldsymbol{\beta}}^{(k)})^{\top} U^{(k)} + \frac{1}{2}\gamma_k(\boldsymbol{\beta}^{(k)} - \widetilde{\boldsymbol{\beta}}^{(k)})^{\top}(\boldsymbol{\beta}^{(k)} - \widetilde{\boldsymbol{\beta}}^{(k)}) + \lambda v_k \|\boldsymbol{\beta}^{(k)}\|_2. \quad (2.31)$$

Let $\widetilde{\boldsymbol{\beta}}^{(k)}(\text{new})$ be the solution to (2.31) which has a simple closed-from expression:

$$\widetilde{\boldsymbol{\beta}}^{(k)}(\text{new}) = \frac{1}{\gamma_k}\left(U^{(k)} + \gamma_k\widetilde{\boldsymbol{\beta}}^{(k)}\right)\left(1 - \frac{\lambda v_k}{\|U^{(k)} + \gamma_k\widetilde{\boldsymbol{\beta}}^{(k)}\|_2}\right)_+. \quad (2.32)$$

Algorithm 3 summarizes the details of GMD for the group lasso with least-squares loss function given by (2.24). The GMD algorithm has the strict descent property and converges to the right answer. The proof follows directly from Section 3.1 of Y. Yang & Zou (2015).
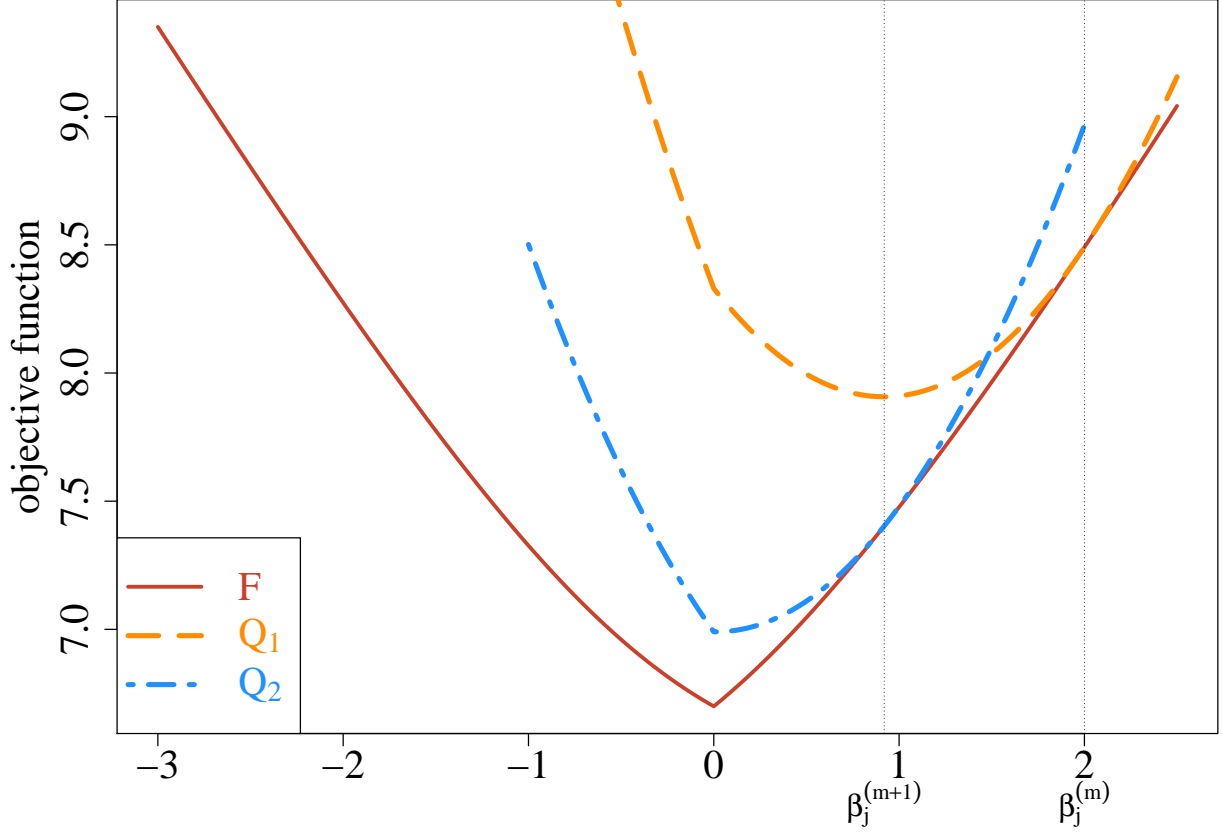
Figure 2.2: Illustration of the quadratic majorization technique

In Figure 2.2 we provide an illustration of the quadratic majorization technique for updating a parameter β_j. The solution lies at the minimum of the F curve but we cannot solve for this directly since there is no closed form solution. Instead we majorize F using Q_1 which is a function consisting of the quadratic approximation of F plus the penalty term evaluated at $\beta_j^{(m)}$. The minimum of Q_1, for which there is a closed form solution, corresponds to the next iteration $\beta_j^{(m+1)}$. We then majorize again using Q_2 and solve for the minimum. This process is repeated until convergence.

2.3.2 Lambda sequence

Similar to Section 2.2.2, we compute the solution to (2.23) over a decreasing sequence of values for the tuning parameter λ starting with λ_{max}. From the update formula (2.32) we

Algorithm 3: The GMD algorithm for group lasso with least-squares loss function given by (2.24).

1. For $k = 1, \ldots, K$, compute γ_k, the largest eigenvalue of $\mathbf{H}^{(k)} = (\mathbf{X}^{(k)})^\top \mathbf{W} \mathbf{X}^{(k)}$
2. Initialize $\widetilde{\boldsymbol{\beta}}$.
3. Repeat the following cyclic groupwise updates until convergence:
   — for $k = 1, \ldots, K$, do step (3.1)–(3.3)
   3.1 Compute $U(\widetilde{\boldsymbol{\beta}}) = -\nabla L(\widetilde{\boldsymbol{\beta}}|\mathbf{D}) = -(\boldsymbol{y} - \hat{\boldsymbol{y}})^\top \mathbf{W} \mathbf{X}^{(k)}$
   3.2 Compute $\widetilde{\boldsymbol{\beta}}^{(k)}(\text{new}) = \frac{1}{\gamma_k} \left(U^{(k)} + \gamma_k \widetilde{\boldsymbol{\beta}}^{(k)} \right) \left(1 - \frac{\lambda v_k}{\|U^{(k)} + \gamma_k \widetilde{\boldsymbol{\beta}}^{(k)}\|_2} \right)_+$.
   3.3 Set $\widetilde{\boldsymbol{\beta}}^{(k)} = \widetilde{\boldsymbol{\beta}}^{(k)}(\text{new})$.

have that for all k

$$
\begin{cases}
\widetilde{\boldsymbol{\beta}}^{(k)} = \frac{1}{\gamma_k} \left(U^{(k)} + \gamma_k \widetilde{\boldsymbol{\beta}}^{(k)} \right) \left(1 - \frac{\lambda v_k}{\|U^{(k)} + \gamma_k \widetilde{\boldsymbol{\beta}}^{(k)}\|_2} \right) & \text{if } \|U^{(k)} + \gamma_k \widetilde{\boldsymbol{\beta}}^{(k)}\|_2 > \lambda v_k \\
\widetilde{\boldsymbol{\beta}}^{(k)} = \mathbf{0} & \text{if } \|U^{(k)} + \gamma_k \widetilde{\boldsymbol{\beta}}^{(k)}\|_2 \le \lambda v_k \ .
\end{cases}
$$

We can then directly obtain the KKT conditions for $k = 1, \ldots, K$:

$$
-U^{(k)} + \lambda v_k \cdot \frac{\widetilde{\boldsymbol{\beta}}^{(k)}}{\|\widetilde{\boldsymbol{\beta}}^{(k)}\|_2} = \mathbf{0} \qquad \text{if } \widetilde{\boldsymbol{\beta}}^{(k)} \ne \mathbf{0},
$$

$$
\|U^{(k)}\|_2 \le \lambda w_k \qquad \text{if } \widetilde{\boldsymbol{\beta}}^{(k)} = \mathbf{0} \ .
$$

$$(2.33)$$

Using (2.33) we can solve for the smallest value of λ such that the entire vector $\left\{ \widehat{\boldsymbol{\beta}}^{(k)} \right\}_{k=1}^K$ is 0. This is given by

$$
\lambda_{max} = \max_k \frac{1}{v_k} \|U^{(k)}\|_2, \quad k = 1, \ldots, K, \ v_k \ne 0
$$

$$(2.34)$$

2.3.3 Warm starts and adaptive group lasso

Warm starts can also be implemented for the group lasso as described in Section 2.2.3 for the lasso. Furthermore, the adaptive group lasso can be computed using Algorithm 2; the

main difference is that the coefficient estimates in Step 1 are obtained from a group lasso fit and the weights for group k are given by $v_k = \left(\left\| \widehat{\boldsymbol{\beta}}^{(k)} \right\|_2 \right)^{-1}$.

2.4 Penalized interaction models

In this section, we introduce penalized regression methods in the context of interaction models. We consider a regression model for an n-length outcome variable $\boldsymbol{y}$ which follows an exponential family. Let $E = (e_1, \ldots, e_n)$ be the binary environment or exposure vector and $\mathbf{X}$ the $n \times p$ matrix of high-dimensional data. Consider the regression model with main effects and their interactions with E:

$$g(\boldsymbol{\mu}) = \beta_0 + \underbrace{\beta_1 X_1 + \cdots + \beta_p X_p + \beta_E E}_{\text{main effects}} + \underbrace{\alpha_{1E}(X_1 E) + \cdots + \alpha_{pE}(X_p E)}_{\text{interactions}} \tag{2.35}$$

where $g(\cdot)$ is a known link function and $\boldsymbol{\mu} = \mathsf{E}\left[\boldsymbol{y}|\mathbf{X}, E, \boldsymbol{\beta}, \boldsymbol{\alpha}\right]$. Due to the large number of parameters to estimate with respect to the number of observations, we might consider adding the lasso penalty introduced in Section 2.2. A natural extension of the lasso penalty applied to the interaction model (2.35) is

$$\arg\min_{\beta_0, \boldsymbol{\beta}, \boldsymbol{\alpha}} \frac{1}{2} \|Y - g(\boldsymbol{\mu})\|_2^2 + \lambda \left(\|\boldsymbol{\beta}\|_1 + \|\boldsymbol{\alpha}\|_1 \right) , \tag{2.36}$$

where $\|Y - g(\boldsymbol{\mu})\|_2^2 = \sum_i (y_i - g(\mu_i))^2$, $\|\boldsymbol{\beta}\|_1 = \sum_j |\beta_j|$, $\|\boldsymbol{\alpha}\|_1 = \sum_j |\alpha_j|$ and $\lambda \geq 0$ is the tuning parameter that can set some of the coefficients to zero when sufficiently large. A limitation of (2.36) is that the selected model may have main effects that are 0 but the corresponding interaction terms are not. This is due to the penalty which treats both main effects and interactions equally. While there may exist situations where this can occur, statisticians have long argued that large main effects are more likely to lead to detectable interactions than small ones (Cox, 1984) and therefore, main effects should enter the model

before interactions. This is known as the strong heredity principle (Chipman, 1996):

$$\hat{\alpha}_{jE} \neq 0 \qquad \Rightarrow \qquad \hat{\beta}_j \neq 0 \qquad \text{and} \qquad \hat{\beta}_E \neq 0 \tag{2.37}$$

In words, the interaction term will only have a non-zero estimate if its corresponding main effects are estimated to be non-zero. One benefit brought by hierarchy is that the number of measured variables can be reduced, referred to as practical sparsity (Bien et al., 2013; She & Jiang, 2014). For example, a model involving $X_1, E, X_1 \cdot E$ is more parsimonious than a model involving $X_1, E, X_2 \cdot E$, because in the first model a researcher would only have to measure two variables compared to three in the second model.

There have been several proposals for modeling interactions with the strong heredity constraint in the penalization literature including Composite Absolute Penalties (CAP) (Zhao et al., 2009), Variable selection using Adaptive Nonlinear Interaction Structures in High dimensions (VANISH) (Radchenko & James, 2010), Strong Hierarchical Lasso (hierNet) (Bien et al., 2013), Group-Lasso Interaction Network (glinternet) (Lim & Hastie, 2015), Group Regularized Estimation under Structural Hierarchy (GRESH) (She & Jiang, 2014) and a Framework for Modeling Interactions with a Convex Penalty (FAMILY) (Haris et al., 2014). A popular approach to achieve this structured sparsity is via the group lasso penalty where each group contains both main effects and their corresponding interactions. For example, consider a two-way interaction model of the form

$$\begin{aligned} y = & \beta_0 + \beta_1 X_1 + \beta_2 X_2 + \beta_3 X_3 \\ & + \beta_{12} X_1 X_2 + \beta_{13} X_1 X_3 + \beta_{23} X_2 X_3 + \varepsilon \end{aligned}$$

A grouping structure that would satisfy the strong heredity property is:

group	1	2	3	4			5			6		
parameter	β_1	β_2	β_3	β_1	β_2	β_{12}	β_1	β_3	β_{13}	β_2	β_3	β_{23}

A limitation of this approach is that its impossible to select one variable without selecting all the groups containing it (Jacob et al., 2009). This implies that if a main effect has been selected, all the interaction terms with that main effect will necessarily be selected as well which can be an issue when the truth contains no interactions.

In Chapter 3 of the thesis, we introduce a new structured sparsity called `sail` which satisfies the strong heredity property while overcoming this issue, i.e., a selected main effect does not automatically imply that the corresponding interactions will also be selected. Furthermore, our method can accommodate non-linear interaction effects on the response. The context of Chapter 3 is summarized in Table 2.1.

Table 2.1: Overview of methods with structured sparsity for penalized regression models

Type	Method	Software
Linear	`CAP` (Zhao et al., 2009)	✗
	`SHIM` (Choi et al., 2010)	✗
	`hiernet` (Bien et al., 2013)	`hierNet(x, y)`
	`GRESH` (She & Jiang, 2014)	✗
	`FAMILY` (Haris et al., 2016)	`FAMILY(x, z, y)`
	`glinternet` (Lim & Hastie, 2015)	`glinternet(x, y)`
	`RAMP` (Hao et al., 2018)	`RAMP(x, y)`
	`LassoBacktracking` (Shah, 2016)	`LassoBT(x, y)`
Non-linear	`VANISH` (Radchenko & James, 2010)	✗
	`sail` (Chapter 3 of the thesis)	`sail(x, y, e)`

2.5 Linear mixed-effects models

Linear mixed-effects models (LMMs) (Laird & Ware, 1982) are a class of statistical models used to account for correlations induced by a natural grouping of the observations such as

students in schools or repeated measurements on the same individual. By introducing a subject specific random effect, LMMs can simultaneously model the mean and covariance structure to produce valid standard errors. In this section we briefly introduce LMMs as a preface to Chapter 4 of the thesis which is about penalized LMMs.

Let $i = 1, \ldots, N$ be the grouping index, $j = 1, \ldots, n_i$ the observation index within a group and $N_T = \sum_{i=1}^{N} n_i$ the total number of observations. For each group let $\boldsymbol{y}_i = (y_1, \ldots, y_{n_i})$ be the observed vector of responses, $\mathbf{X}_i$ an $n_i \times (p+1)$ design matrix (with the column of 1s for the intercept), $\boldsymbol{b}_i$ a group-specific random effect vector of length n_i and $\boldsymbol{\varepsilon}_i = (\varepsilon_{i1}, \ldots, \varepsilon_{in_i})$ the individual error terms. Denote the stacked vectors $\mathbf{Y} = (\boldsymbol{y}_i, \ldots, \boldsymbol{y}_N)^T \in \mathbb{R}^{N_T \times 1}$, $\boldsymbol{b} = (\boldsymbol{b}_i, \ldots, \boldsymbol{b}_N)^T \in \mathbb{R}^{N_T \times 1}$, $\boldsymbol{\varepsilon} = (\boldsymbol{\varepsilon}_i, \ldots, \boldsymbol{\varepsilon}_N)^T \in \mathbb{R}^{N_T \times 1}$, and the stacked matrix $\mathbf{X} = (\mathbf{X}_1, \ldots, \mathbf{X}_N)^T \in \mathbb{R}^{N_T \times (p+1)}$. Furthermore, let $\boldsymbol{\beta} = (\beta_0, \beta_1, \ldots, \beta_p)^T \in \mathbb{R}^{(p+1) \times 1}$ be a vector of fixed effects regression coefficients corresponding to $\mathbf{X}$. We consider the following LMM with a single random effect:

$$\mathbf{Y} = \mathbf{X}\boldsymbol{\beta} + \boldsymbol{b} + \boldsymbol{\varepsilon} \tag{2.38}$$

where the random effect $\boldsymbol{b}$ and the error variance $\boldsymbol{\varepsilon}$ are assigned the distributions

$$\boldsymbol{b} \sim \mathcal{N}(0, \eta\sigma^2 \boldsymbol{\Phi}) \qquad \boldsymbol{\varepsilon} \sim \mathcal{N}(0, (1-\eta)\sigma^2 \mathbf{I}) \tag{2.39}$$

Here, $\boldsymbol{\Phi}_{N_T \times N_T}$ is a known positive semi-definite and symmetric covariance matrix, $\mathbf{I}_{N_T \times N_T}$ is the identity matrix and parameters σ^2 and $\eta \in [0, 1]$ determine how the variance is divided between $\boldsymbol{b}$ and $\boldsymbol{\varepsilon}$. The joint density of $\mathbf{Y}$ is multivariate normal:

$$\mathbf{Y} | (\boldsymbol{\beta}, \eta, \sigma^2) \sim \mathcal{N}(\mathbf{X}\boldsymbol{\beta}, \eta\sigma^2 \boldsymbol{\Phi} + (1-\eta)\sigma^2 \mathbf{I}) \tag{2.40}$$

In high-dimensional contexts, the classic LMM is no longer applicable for the same reasons why the linear model does not apply, i.e., singularity of $\mathbf{X}^T \mathbf{X}$. However, naively applying

a penalized method such as the lasso to clustered data is also invalid. Indeed, ignoring the grouping structure can lead to incorrect inference due to biased standard errors of parameters, and can also violate the normality of residuals assumption. In Chapter 4 of this thesis, we develop a general framework for penalized mixed models that simultaneously performs variable selection while accounting for the correlations induced by the natural clustering of the observations.

Chapter 3

An analytic approach for interpretable predictive models in high dimensional data, in the presence of interactions with exposures

Sahir Rai Bhatnagar[1,2], Yi Yang[3], Budhachandra Khundrakpam[4], Alan C Evans[4], Mathieu Blanchette[5], Luigi Bouchard[6], Celia MT Greenwood[1,2]

[1]Department of Epidemiology, Biostatistics and Occupational Health, McGill University

[2]Lady Davis Institute, Jewish General Hospital, Montréal, QC

[3]Department of Mathematics and Statistics, McGill University

[4]Montreal Neurological Institute, McGill University

[5]Department of Computer Science, McGill University

[6]Department of Biochemistry, Université de Sherbrooke

Abstract

Predicting a phenotype and understanding which variables improve that prediction are two very challenging and overlapping problems in analysis of high-dimensional data such as those arising from genomic and brain imaging studies. It is often believed that the number of truly important predictors is small relative to the total number of variables, making computational approaches to variable selection and dimension reduction extremely important. To reduce dimensionality, commonly-used two-step methods first cluster the data in some way, and build models using cluster summaries to predict the phenotype.

It is known that important exposure variables can alter correlation patterns between clusters of high-dimensional variables, i.e., alter network properties of the variables. However, it is not well understood whether such altered clustering is informative in prediction. Here, assuming there is a binary exposure with such network-altering effects, we explore whether use of exposure-dependent clustering relationships in dimension reduction can improve predictive modelling in a two-step framework. Hence, we propose a modelling framework called ECLUST to test this hypothesis, and evaluate its performance through extensive simulations.

With ECLUST, we found improved prediction and variable selection performance compared to methods that do not consider the environment in the clustering step, or to methods that use the original data as features. We further illustrate this modelling framework through the analysis of three data sets from very different fields, each with high dimensional data, a binary exposure, and a phenotype of interest. Our method is available in the *eclust* CRAN package.

3.1 Introduction

In this article, we consider the prediction of an outcome variable y observed on n individuals from p variables, where p is much larger than n. Challenges in this high-dimensional context include not only building a good predictor which will perform well in an independent dataset, but also being able to interpret the factors that contribute to the predictions. This latter issue can be very challenging in ultra-high dimensional predictor sets. For example, multiple different sets of covariates may provide equivalent measures of goodness of fit (Fan et al., 2014), and therefore how does one decide which are important? If many variables are highly correlated, interpretation may be improved by acknowledging the existence of an underlying or latent factor generating these patterns. In consequence, many authors have suggested a two-step procedure where the first step is to cluster or group variables in the design matrix in an interpretable way, and then to perform model fitting in the second step using a summary measure of each group of variables.

There are several advantages to these two-step methods. Through the reduction of the dimension of the model, the results are often more stable with smaller prediction variance, and through identification of sets of correlated variables, the resulting clusters can provide an easier route to interpretation. From a practical point of view, two-step approaches are both flexible and easy to implement because efficient algorithms exist for both clustering (e.g. (Müllner, 2013)) and model fitting (e.g. (J. Friedman et al., 2010; Kuhn, 2008; Y. Yang & Zou, 2014)), particularly in the case when the outcome variable is continuous.

This two-step idea dates back to 1957 when Kendall first proposed using principal components in regression (Kendall, 1957). Hierarchical clustering based on the correlation of the design matrix has also been used to create groups of genes in microarray studies. For example, at each level of a hierarchy, cluster averages have been used as new sets of potential predictors in both forward-backward selection (Hastie et al., 2001) or the lasso (Park et al., 2007). Bühlmann *et al.* proposed a bottom-up agglomerative clustering algorithm based on

canonical correlations and used the group lasso on the derived clusters (Bühlmann et al., 2013). A more recent proposal performs sparse regression on cluster prototypes (Reid & Tibshirani, 2016), i.e., extracting the most representative gene in a cluster instead of averaging them.

These two-step approaches usually group variables based on a matrix of correlations or some transformation of the correlations. However, when there are external factors, such as exposures, that can alter correlation patterns, a dimension reduction step that ignores this information may be suboptimal. Many of the high-dimensional genomic data sets currently being generated capture a possibly dynamic view of how a tissue is functioning, and demonstrate differential patterns of coregulation or correlation under different conditions. We illustrate this critical point with an example of a microarray gene expression dataset available in the *COPDSexualDimorphism.data* package (Sathirapongsasuti, 2013) from Bioconductor. This study measured gene expression in Chronic Obstructive Pulmonary Disease (COPD) patients and controls in addition to their age, gender and smoking status. To see if there was any effect of smoking status on gene expression, we plotted the expression profiles separately for current and never smokers. To balance the covariate profiles, we matched subjects from each group on age, gender and COPD case status, resulting in a sample size of 7 in each group. Heatmaps in Figure 3.1 show gene expression levels and the corresponding gene-gene correlation matrices as a function of dichotomized smoking status for 2,900 genes with large variability. Evidently, there are substantial differences in correlation patterns between the smoking groups (Figures 1a and 1b). However, it is difficult to discern any patterns or major differences between the groups when examining the gene expression levels directly (Figures 1c and 1d). This example highlights two key points; 1) environmental exposures can have a widespread effect on regulatory networks and 2) this effect may be more easily discerned by looking at a measure for gene similarity, relative to analyzing raw expression data.

Many other examples of altered co-regulation and phenotype associations can be found. For

(a) Correlations: Never Smokers

(b) Correlations: Current Smokers

(c) Gene Expression: Never Smokers

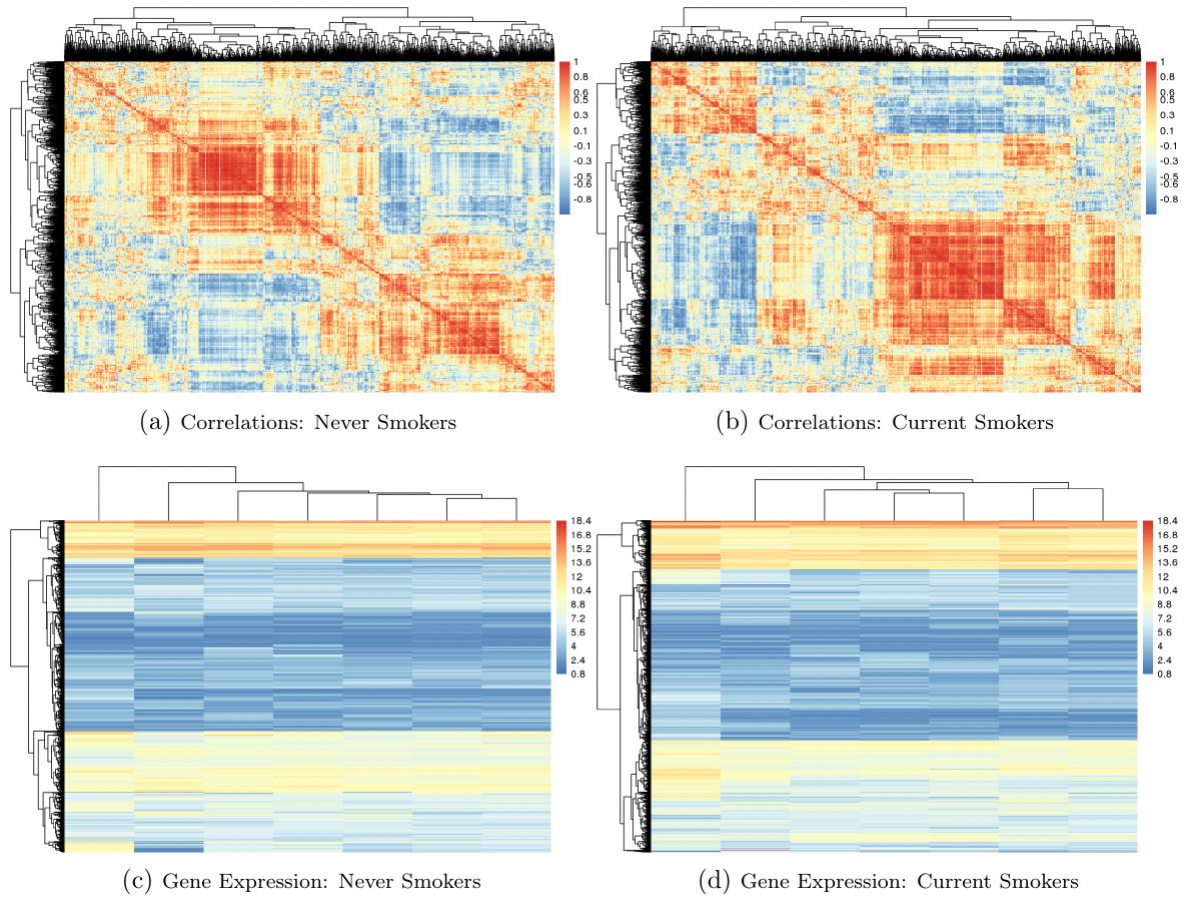(d) Gene Expression: Current Smokers

Figure 3.1: Heatmaps of correlations between genes (top) and gene expression data (bottom - rows are genes and columns are subjects), stratified by smoking status from a microarray study of COPD (Sathirapongsasuti, 2013). The 20% most variable genes are displayed (2,900 genes). There are 7 subjects in each group, matched on COPD case status, gender and age. Data available on Bioconductor in the COPDSexualDimorphism.data package.

instance, in a pediatric brain development study, very different correlation patterns of cortical thickness within brain regions were observed across age groups, consistent with a process of fine-tuning an immature brain system into a mature one (Khundrakpam et al., 2013). A comparison of gene expression levels in bone marrow from 327 children with acute leukemia found several differentially *coexpressed* genes in philadelphia positive leukemias compared to the cytogenetically normal group (Kostka & Spang, 2004). To give a third example, an analysis of RNA-sequencing data from The Cancer Genome Atlas (TCGA) revealed very different correlation patterns among sets of genes in tumors grouped according to their missense or null mutations in the TP53 tumor suppressor gene (Klein et al., 2016).

Therefore, in this paper, we pose the question whether clustering or dimension reduction that incorporates known covariate or exposure information can improve prediction models in high dimensional genomic data settings. Substantial evidence of dysregulation of genomic coregulation has been observed in a variety of contexts, however we are not aware of any work that carefully examines how this might impact the performance of prediction models. We propose a conceptual analytic strategy called ECLUST, for prediction of a continuous or binary outcome in high dimensional contexts while exploiting exposure-sensitive data clusters. We restrict our attention to two-step algorithms in order to implement a covariate-driven clustering.

Specifically, we hypothesize that within two-step methods, variable grouping that considers exposure information can lead to improved predictive accuracy and interpretability. We use simulations to compare our proposed method to comparable approaches that combine data reduction with predictive modelling. We are focusing our attention primarily on the performance of alternative dimension reduction strategies within the first step of a two-step method. Therefore, performance of each strategy is compared for several appropriate step 2 predictive models. We then illustrate these concepts more concretely by analyzing three data sets. Our method and the functions used to conduct the simulation studies have been

implemented in the R package `eclust` (Bhatnagar, 2017), available on CRAN. Extensive documentation of the package is available at http://sahirbhatnagar.com/eclust/.

3.2 Methods

Assume there is a single binary environmental factor E of importance, and an $n \times p$ high dimensional (HD) data set $\mathbf{X}$ (n observations, p features) of relevance. This could be genome-wide epigenetic data, gene expression data, or brain imaging data, for example. Assume there is a continuous or binary phenotype of interest Y and that the environment has a widespread effect on the HD data, i.e., affects many elements of the HD data. The primary goal is to improve prediction of Y by identifying interactions between E and $\mathbf{X}$ through a carefully constructed data reduction strategy that exploits E dependent correlation patterns. The secondary goal is to improve identification of the elements of $\mathbf{X}$ that are involved; we denote this subset by S_0. We hypothesize that a systems-based perspective will be informative when exploring the factors that are associated with a phenotype of interest, and in particular we hypothesize that incorporation of environmental factors into predictive models in a way that retains a high dimensional perspective will improve results and interpretation.

3.2.1 Potential impacts of covariate-dependent coregulation

Motivated by real world examples of differential coexpression, we first demonstrate that environment-dependent correlations in $\boldsymbol{x}$ can induce an interaction model. Without loss of generality, let $p = 2$ and the relationship between X_1 and X_2 depend on the environment such that

$$X_{i2} = \psi X_{i1} E_i + \varepsilon_i \tag{3.1}$$

where ε_i is an error term and ψ is a slope parameter, that is:

$$X_{i2} = \begin{cases} \psi X_{i1} + \varepsilon_i & \text{when } E_i = 1 \\ \\ \varepsilon_i & \text{when } E_i = 0 \end{cases}$$

Consider the 3-predictor regression model

$$Y_i = \beta_0 + \beta_1 X_{i1} + \beta_2 X_{i2} + \beta_3 E_i + \varepsilon_i^* \tag{3.2}$$

where ε_i^* is another error term which is independent of ε_i. At first glance (3.2) does not contain any interaction terms. However, substituting (3.1) for X_{i2} in (3.2) we get

$$Y_i = \beta_0 + \beta_1 X_{i1} + \beta_2 \psi \left(X_{i1} E_i \right) + \beta_3 E_i + \varepsilon_i \beta_2 + \varepsilon_i^* \tag{3.3}$$

The third term in (3.3) resembles an interaction model, with $\beta_2 \psi$ being the interaction parameter. We present a second illustration showing how non-linearity can induce interactions. Suppose

$$Y_i = \beta_0 + \beta_1 X_{i1} + \beta_2 X_{i2} + \beta_3 E_i + \beta_3 \max_{j \in \{1,2\}} \left(X_{ij} - \bar{X}_i \right)^2 + \varepsilon_i^* \tag{3.4}$$

Substituting (3.1) for X_{i2} in (3.4) we obtain a non-linear interaction term. Equation (3.4) provided partial motivation for the model used in our third simulation scenario. Some motivation for this model and a graphical representation are presented below in the Simulation Studies section.

3.2.2 Proposed framework and algorithm

We restrict attention to methods containing two phases as illustrated in Figure 3.2: 1a) a clustering stage where variables are clustered based on some measure of similarity, 1b) a
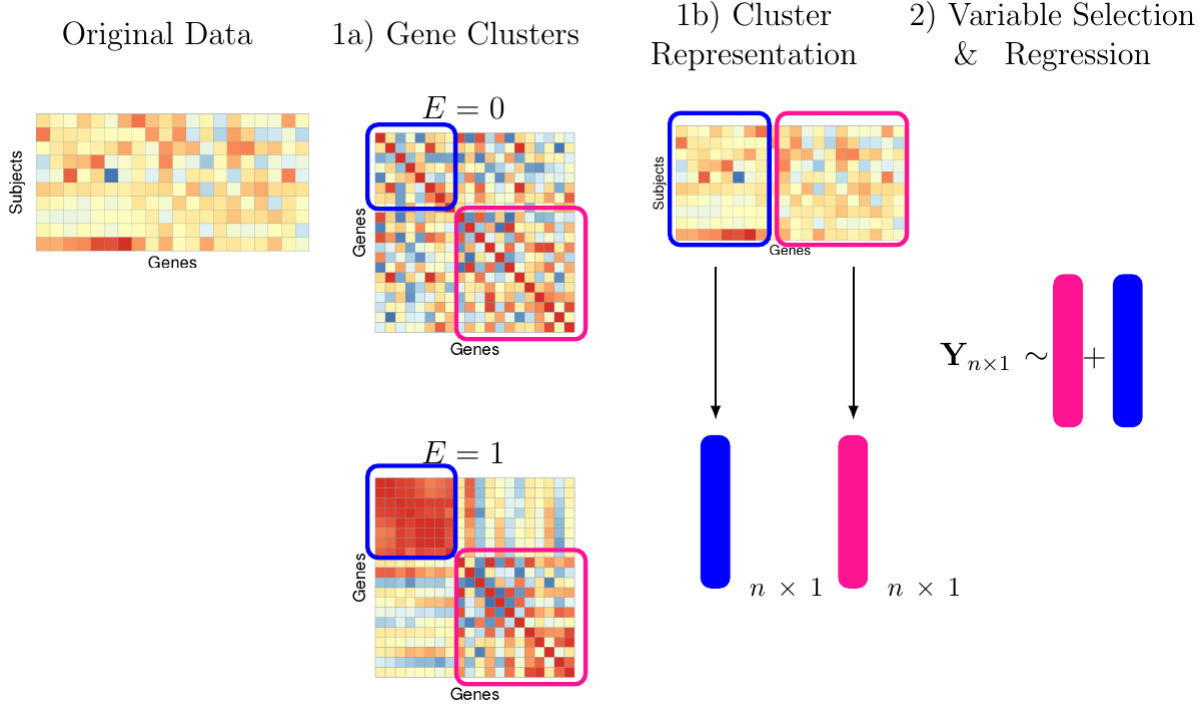
Figure 3.2: Overview of our proposed method. 1a) A measure of similarity is calculated separately for both groups and clustering is performed on a linear combination of these two matrices. 1b) We reduce the dimension of each cluster by taking a summary measure. 2) Variable selection and regression is performed on the cluster representatives, E and their interaction with E.

dimension reduction stage where a summary measure is created for each of the clusters, and 2) a simultaneous variable selection and regression stage on the summarized cluster measures. Although this framework appears very similar to any two-step approach, our hypothesis is that allowing the clustering in Step 1a to depend on the environment variable can lead to improvements in prediction after Step 2. Hence, methods in Step 1a are adapted to this end, as decribed in the following sections. Our focus in this manuscript is on the clustering and cluster representation steps. Therefore, we compare several well known methods for variable selection and regression that are best adapted to our simulation designs and data sets.

Step 1a: Clustering using co-expression networks that are influenced by the environment

In agglomerative clustering, a measure of similarity between sets of observations is required in order to decide which clusters should be combined. Common choices include Euclidean, maximum and absolute distance. A more natural choice in genomic or brain imaging data is to use Pearson correlation (or its absolute value) because the derived clusters are biologically interpretable. Indeed, genes that cluster together are correlated and thus likely to be involved in the same cellular process. Similarly, cortical thickness measures of the brain tend to be correlated within pre-defined regions such as the left and right hemisphere, or frontal and temporal regions (Sato et al., 2013). However, the information on the connection between two variables, as measured by the Pearson correlation for example, may be noisy or incomplete. Thus it is of interest to consider alternative measures of pairwise interconnectedness. Gene co-expression networks are being used to explore the system-level function of genes, where nodes represent genes and are connected if they are significantly co-expressed (B. Zhang & Horvath, 2005), and here we use their overlap measure (Ravasz et al., 2002) to capture connectnedness between two X variables within each environmental condition. As was discussed earlier, genes can exhibit very different patterns of correlation in one environment versus the other (e.g. Figure 3.1). Furthermore, measures of similarity that go beyond pairwise correlations and consider the shared connectedness between nodes can be useful in elucidating networks that are biologically meaningful. Therefore, we propose to first look at the topological overlap matrix (TOM) separately for exposed ($E = 1$) and unexposed ($E = 0$) individuals (see Supplemental Section A for details on the TOM). We then seek to identify nodes that are very different between environments. We determine differential coexpression using the absolute difference $TOM(X_{\text{diff}}) = |TOM_{E=1} - TOM_{E=0}|$ (Klein et al., 2016). We then use hierarchical clustering with average linkage on the derived difference matrix to identify these differentially co-expressed variables. Clusters are auto-

matically chosen using the `dynamicTreeCut` (Langfelder et al., 2008) algorithm. Of course, there could be other clusters which are not sensitive to the environment. For this reason we also create a set of clusters based on the TOM for all subjects denoted $TOM(X_{\text{all}})$. This will lead to each covariate appearing in two clusters. In the sequel we denote the clusters derived from $TOM(X_{\text{all}})$ as the set $C_{\text{all}} = \{C_1, \ldots, C_k\}$, and those derived from $TOM(X_{\text{diff}})$ as the set $C_{\text{diff}} = \{C_{k+1}, \ldots, C_\ell\}$ where $k < \ell < p$.

Step 1b: Dimension reduction via cluster representative

Once the clusters have been identified in phase 1, we proceed to reduce the dimensionality of the overall problem by creating a summary measure for each cluster. A low-dimensional structure, i.e. grouping when captured in a regression model, improves predictive performance and facilitates a model's interpretability. We propose to summarize a cluster by a single representative number. Specifically, we chose the average values across all measures (Bühlmann et al., 2013; Park et al., 2007), and the first principal component (Langfelder & Horvath, 2007). These representative measures are indexed by their cluster, i.e., the variables to be used in our predictive models are $\widetilde{\mathbf{X}}_{\text{all}} = \left\{ \widetilde{X}_{C_1}, \ldots, \widetilde{X}_{C_k} \right\}$ for clusters that do not consider E, as well as $\widetilde{\mathbf{X}}_{\text{diff}} = \left\{ \widetilde{X}_{C_{k+1}}, \ldots, \widetilde{X}_{C_\ell} \right\}$ for E-derived clusters. The tilde notation on the X is to emphasize that these variables are different from the separate variables in the original data.

Step 2: Variable Selection and Regression

Because the clustering in phase 1 is unsupervised, it is possible that the derived latent representations from phase 2 will not be associated with the response. We therefore use penalized methods for supervised variable selection, including the lasso (Tibshirani, 1996) and elasticnet (Zou & Hastie, 2005) for linear models, and multivariate adaptive regression splines (MARS) (J. H. Friedman, 1991) for nonlinear models. We argue that the selected

non-zero predictors in this model will represent clusters of genes that interact with the environment and are associated with the phenotype. Such an additive model might be insufficient for predicting the outcome. In this case we may directly include the environment variable, the summary measures and their interaction. In the light of our goals to improve prediction and interpretability, we consider the following model

$$g(\boldsymbol{\mu}) = \beta_0 + \sum_{j=1}^{\ell} \beta_j \widetilde{X}_{C_j} + \beta_E E + \sum_{j=1}^{\ell} \alpha_j \left(\widetilde{X}_{C_j} E \right) + \varepsilon \tag{3.5}$$

where $g(\cdot)$ is a known link function, $\boldsymbol{\mu} = \mathsf{E}[Y|\mathbf{X}, E, \boldsymbol{\beta}, \boldsymbol{\alpha}]$ and $\widetilde{X}_{C_j}$ are linear combinations of $\mathbf{X}$ (from Step 1b). The primary comparison is models with $\widetilde{\mathbf{X}}_{\mathrm{all}}$ only versus models with $\widetilde{\mathbf{X}}_{\mathrm{all}}$ and $\widetilde{\mathbf{X}}_{\mathrm{diff}}$. Given the context of either the simulation or the data set, we use either linear models or non linear models. Our general approach, ECLUST, can therefore be summarized by the algorithm in Table 3.1.

3.3   Simulation Studies

We have evaluated the performance of our ECLUST method in a variety of simulated scenarios. For each simulation scenario we compared ECLUST to the following analytic approaches 1) regression and variable selection is performed on the model which consists of the original variables, E and their interaction with E (SEPARATE), and 2) clustering is performed without considering the environmental exposure followed by regression and variable selection on the cluster representations, E, and their interaction with E (CLUST). A detailed description of the methods being compared is summarized in Table 3.2. We have designed 6 simulation scenarios that illustrate different kinds of relationships between the variables and the response. For all scenarios, we have created high dimensional data sets with p predictors ($p = 5000$), and sample sizes of $n = 200$. We also assume that we have two data sets for each simulation - a training data set where the parameters are estimated, and a testing data

Table 3.1: Details of ECLUST algorithm

Step	Description, Software[a] and Reference
1a)	i) Calculate TOM separately for observations with $E = 0$ and $E = 1$ using `WGCNA::TOMsimilarityFromExpr` (Langfelder & Horvath, 2008) ii) Euclidean distance matrix of $|TOM_{E=1} - TOM_{E=0}|$ using `stats::dist` iii) Run the `dynamicTreeCut` algorithm (Langfelder et al., 2008, 2016) on the distance matrix to determine the number of clusters and cluster membership using `dynamicTreeCut::cutreeDynamic` with `minClusterSize = 50`
1b)	i) 1st PC or average for each cluster using `stat::prcomp` or `base::mean` ii) Penalized regression model: create a design matrix of the derived cluster representatives and their interactions with E using `stats::model.matrix` iii) MARS model: create a design matrix of the derived cluster representatives and E
2)	i) For linear models, run penalized regression on design matrix from step 1b) using `glmnet::cv.glmnet` (J. Friedman et al., 2010). Elasticnet mixing parameter `alpha=1` corresponds to the lasso and `alpha=0.5` corresponds to the value we used in our simulations for elasticnet. The tuning parameter `alpha` is selected by minimizing 10 fold cross-validated mean squared error (MSE). ii) For non-linear effects, run MARS on the design matrix from step 1b) using `earth::earth` (Milborrow. Derived from mda:mars by T. Hastie and R. Tibshirani., 2011) with pruning method `pmethod = "backward"` and maximum number of model terms `nk = 1000`. The `degree=1,2` is chosen using 10 fold cross validation (CV), and within each fold the number of terms in the model is the one that minimizes the generalized cross validated (GCV) error.

[a]All functions are implemented in `R` (R Core Team, 2016). The naming convention is as follows: `package_name::package_function`. Default settings used for all functions unless indicated otherwise.

set where prediction performance is evaluated, each of size $n_{train} = n_{test} = 200$. The number of subjects who were exposed ($n_{E=1} = 100$) and unexposed ($n_{E=0} = 100$) and the number of truly associated parameters ($|S_0| = 500$) remain fixed across the 6 simulation scenarios. Let

$$Y = Y^* + k \cdot \varepsilon \tag{3.6}$$

where Y^* is the linear predictor, the error term ε is generated from a standard normal distribution, and k is chosen such that the signal-to-noise ratio $SNR = (Var(Y^*)/Var(\varepsilon))$ is 0.2, 1 and 2 (e.g. the variance of the response variable Y due to ε is $1/SNR$ of the variance of Y due to Y^*).

Table 3.2: Summary of methods used in simulation study

General Approach	Summary Measure of Feature Clusters	Description[a,b]
SEPARATE	NA	Regression of the original predictors $\{X_1, \ldots, X_p\}$ on the response i.e. no transformation of the predictors is being done here
CLUST	1st PC, average	Create clusters of predictors without using the environment variable $\{C_1, \ldots, C_k\}$. Use the summary measure of each cluster as inputs of the regression model.
ECLUST	1st PC, average	Create clusters of predictors using the environment variable $\{C_{k+1}, \ldots, C_\ell\}$ where $k < \ell < p$, as well as clusters without the environment variable $\{C_1, \ldots, C_k\}$. Use summary measures of $\{C_1, \ldots, C_\ell\}$ as inputs of the regression model.

[a]Simulations 1 and 2 used lasso and elasticnet for the linear models, and simulation 3 used MARS for estimating non-linear effects [b]Simulations 4, 5 and 6 convert the continuous response generated in simulations 1, 2 and 3, respectively, into a binary response [c]PC: principal component

3.3.1 The Design Matrix

We generated covariate data in blocks using the `simulateDatExpr` function from the `WGCNA` package in `R` (version 1.51). This generates data from a latent vector: first a seed vector is simulated, then covariates are generated with varying degree of correlation with the seed vector in a given block. We simulated five clusters (blocks), each of size 750 variables, and labeled them by colour (turquoise, blue, red, green and yellow), while the remaining 1250 variables were simulated as independent standard normal vectors (grey) (Figure 3.3). For the unexposed observations ($E = 0$), only the predictors in the yellow block were simulated with correlation, while all other covariates were independent within and between blocks. The TOM values are very small for the yellow cluster because it is not correlated with any of its neighbors. For the exposed observations ($E = 1$), all 5 blocks contained predictors that are correlated. The blue and turquoise blocks are set to have an average correlation of 0.6. The average correlation was varied for both green and red clusters $\rho = \{0.2, 0.9\}$ and

the active set S_0, that are directly associated with y, was distributed evenly between these two blocks. Heatmaps of the TOM for this environment dependent correlation structure are shown in Figure 3.3 with annotations for the true clusters and active variables. This design matrix shows widespread changes in gene networks in the exposed environment, and this subsequently affects the phenotype through the two associated clusters. There are also pathways that respond to changes in the environment but are not associated with the response (blue and turquoise), while others that are neither active in the disease nor affected by the environment (yellow).

3.3.2   The response

The first three simulation scenarios differ in how the linear predictor Y^* in (3.6) is defined, and also in the choice of regression model used to fit the data. In simulations 1 and 2 we use lasso (Tibshirani, 1996) and elasticnet (Zou & Hastie, 2005) to fit linear models; then we use MARS (J. H. Friedman, 1991) in simulation 3 to estimate non-linear effects. Simulations 4, 5 and 6 use the GLM version of these models, respectively, since the responses are binary.

Simulation 1

Simulation 1 was designed to evaluate performance when there are no explicit interactions between X and E (see Equation (3.3)). We generated the linear predictor from

$$Y^* = \sum_{\substack{j \in \{1,\dots,250\} \\ j \in \text{ red, green block}}} \beta_j X_j + \beta_E E \qquad (3.7)$$

where $\beta_j \sim \text{Unif}\,[0.9, 1.1]$ and $\beta_E = 2$. That is, only the first 250 predictors of both the red and green blocks are active. In this setting, only the main effects model is being fit to the simulated data.

(a) $TOM(X_{E=0})$

(b) $TOM(X_{E=1})$

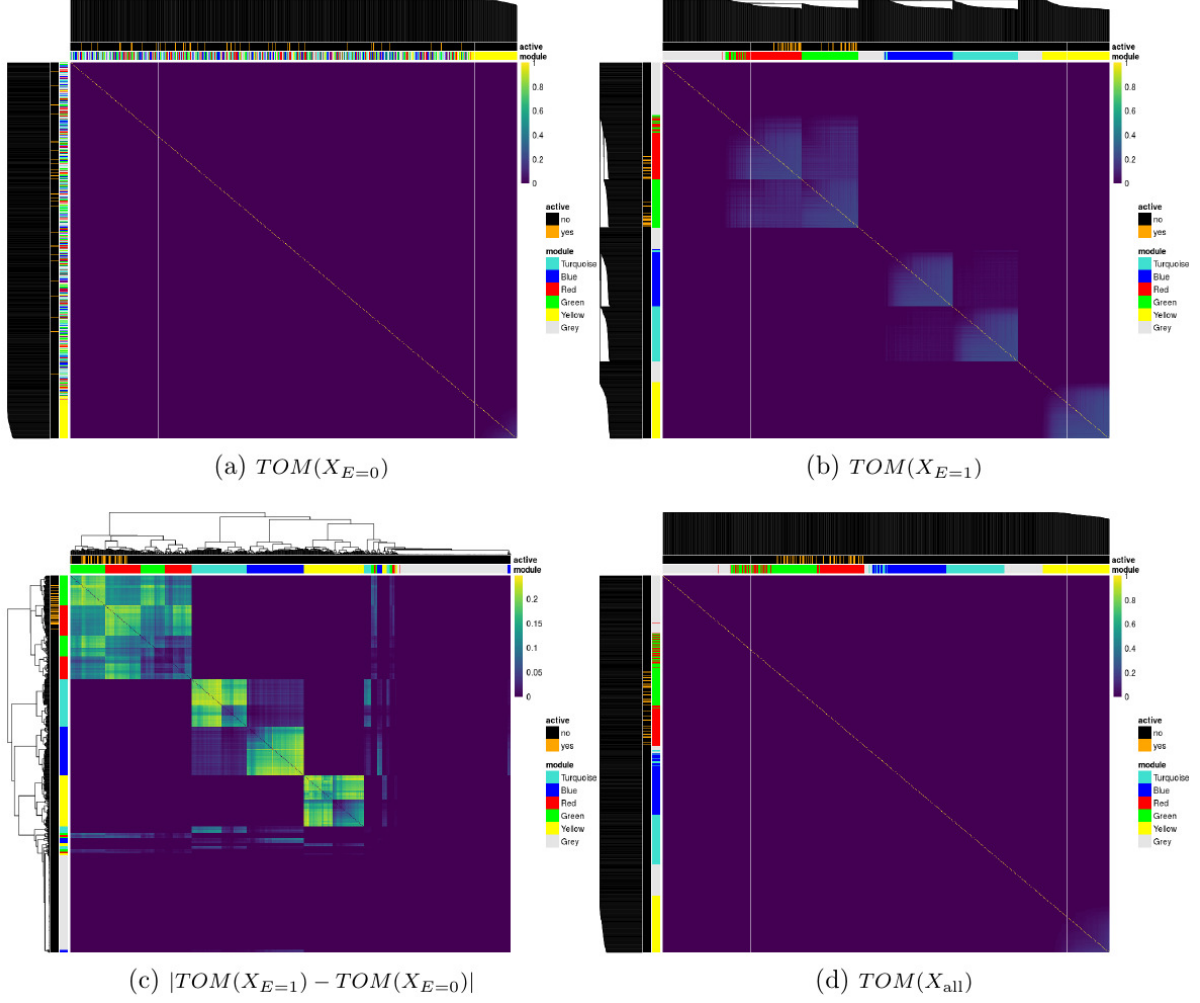(c) $|TOM(X_{E=1}) - TOM(X_{E=0})|$

(d) $TOM(X_{\mathrm{all}})$

Figure 3.3: Topological overlap matrices (TOM) of simulated predictors based on subjects with (a) $E = 0$, (b) $E = 1$, (c) their absolute difference and (d) all subjects. Dendrograms are from hierarchical clustering (average linkage) of one minus the TOM for a, b, and d and the euclidean distance for c. Some variables in the red and green clusters are associated with the outcome variable. The *module* annotation represents the true cluster membership for each predictor, and the *active* annotation represents the truly associated predictors with the response.

Simulation 2

In the second scenario we explicitly simulated interactions. All non-zero main effects also had a corresponding non-zero interaction effect with E. We generated the linear predictor from

$$Y^* = \sum_{\substack{j \in \{1,\ldots,125\} \\ j \in \text{ red, green block}}} \left(\beta_j X_j + \alpha_j X_j E\right) + \beta_E E \tag{3.8}$$

where $\beta_j \sim \text{Unif}\,[0.9, 1.1]$, $\alpha_j \sim \text{Unif}\,[0.4, 0.6]$ or $\alpha_j \sim \text{Unif}\,[1.9, 2.1]$, and $\beta_E = 2$. In this setting, both the main effects and their interactions with E are being fit to the simulated data.

Simulation 3

In the third simulation we investigated the performance of the ECLUST approach in the presence of non-linear effects of the predictors on the phenotype:

$$Y_i^* = \sum_{\substack{j \in \{1,\ldots,250\} \\ j \in \text{ red, green block}}} \beta_j X_{ij} + \beta_E E_i + \alpha_Q E_i \cdot f(Q_i) \tag{3.9}$$

where

$$Q_i = -\max_{\substack{j \in \{1,\ldots,250\} \\ j \in \text{ red, green block}}} \left(X_{ij} - \bar{X}_i\right)^2 \tag{3.10}$$

$$f(u_i) = \frac{u_i - \min\limits_{i \in \{1,\ldots,n\}} u_i}{- \min\limits_{i \in \{1,\ldots,n\}} u_i} \tag{3.11}$$

$$\bar{X}_i = \frac{1}{500} \sum_{\substack{j \in \{1,\ldots,250\} \\ j \in \text{ red, green block}}} X_{ij}$$

The design of this simulation was partially motivated by considering the idea of canalization, where systems operate within appropriate parameters until sufficient perturbations accumu-
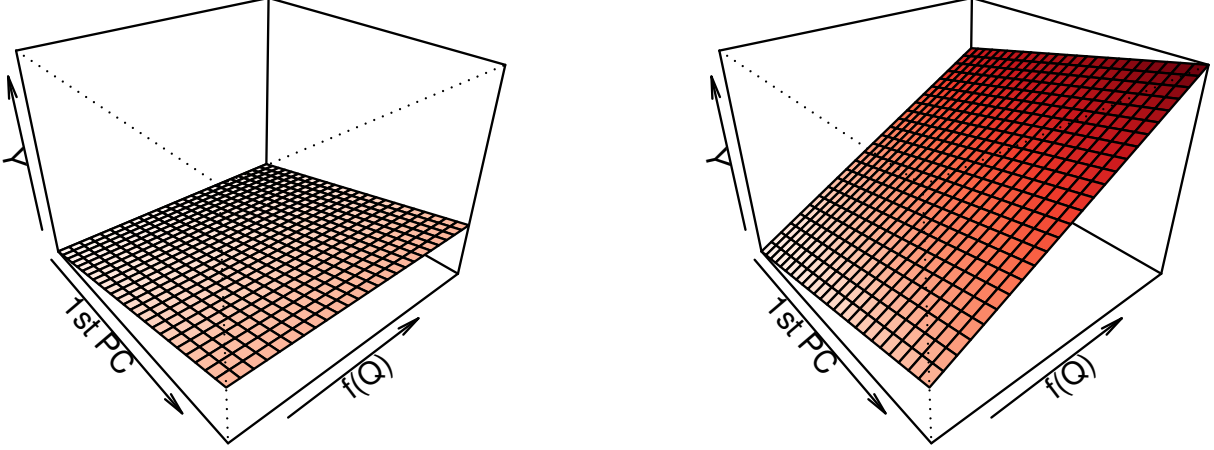
Figure 3.4: Visualization of the relationship between the response, the first principal component of the main effects and $f(Q_i)$ in (3.9) for $E = 0$ (left) and $E = 1$ (right) in simulation scenario 3. This graphic also depicts the intuition behind model (3.4).

late (e.g. Gibson (2009)). In this third simulation, we set $\beta_j \sim \text{Unif}[0.9, 1.1]$, $\beta_E = 2$ and $\alpha_Q = 1$. We assume the data has been appropriately normalized, and that the correlation between any two features is greater than or equal to 0. In simulation 3, we tried to capture the idea that an exposure could lead to coregulation or disregulation of a cluster of X's, which in itself directly impacts Y. Hence, we defined coregulation as the X's being similar in magnitude and disregulation as the X's being very different. The Q_i term in (3.10) is defined such that higher values would correspond to strong coregulation whereas lower values correspond to disregulation. For example, suppose Q_i ranges from -5 to 0. It will be -5 when there is lots of variability (disregulation) and 0 when there is none (strong coregulation). The function $f(\cdot)$ in (3.11) simply maps Q_i to the [0,1] range. In order to get an idea of the relationship in (3.9), Figure 3.4 displays the response Y as a function of the first principal component of $\sum_j \beta_j X_{ij}$ (denoted by 1st PC) and $f(Q_i)$. We see that lower values of $f(Q_i)$ (which implies disregulation of the features) leads to a lower Y. In this setting, although the clusters do not explicitly include interactions between the X variables, the MARS algorithm allows for the possibility of two way interactions between any of the variables.

Simulations 4, 5 and 6

We used the same simulation setup as above, except that we took the continuous outcome Y, defined $p = 1/(1 + exp(-Y))$ and used this to generate a two-class outcome z with $\Pr(z = 1) = p$ and $\Pr(z = 0) = 1 - p$. The true parameters were simulated as $\beta_j \sim$ Unif$[\log(0.9), \log(1.1)]$, $\beta_E = \log(2)$, $\alpha_j \sim$ Unif$[\log(0.4), \log(0.6)]$ or $\alpha_j \sim$ Unif$[\log(1.9), \log(2.1)]$. Simulations 4, 5 and 6 are the binary response versions of simulations 1, 2 and 3, respectively. The larger odds ratio for E compared to the odds ratio for X is motivated by certain environmental factors which are well known to have substantial impacts on disease risks and phenotypes. For example, body mass index has been estimated to explain a large proportion of variation in bone mineral density (BMD) in women (10-20%) (Felson et al., 1993). This can be converted to a slope of 0.31-0.44 assuming variables are standardized, i.e., changes of 0.3-0.4 standard deviations in BMD per standard deviation change in weight. In contrast, the majority of SNPs and rare variants have effect sizes under 0.10 standard deviations on BMD (Kemp et al., 2017).

3.3.3   Measures of Performance

Simulation performance was assessed with measures of model fit, prediction accuracy and feature stability. Several measures for each of these categories, and the specific formulae used are provided in Table 3.3. We simulated both a training data set and a test data set for each simulation: all tuning parameters for model selection were selected using the training sets only. Although most of the measures of model fit were calculated on the test data sets, true positive rate, false positive rate and correct sparsity were calculated on the training set only. The root mean squared error is determined by predicting the response for the test set using the fitted model on the training set. The area under the curve is determined using the trapezoidal rule (Robin et al., 2011). The stability of feature importance is defined as the variability of feature weights under perturbations of the training

set, i.e., small modifications in the training set should not lead to considerable changes in the set of important covariates (Toloşi & Lengauer, 2011). A feature selection algorithm produces a weight (e.g. $\boldsymbol{\beta} = (\beta_1, \ldots, \beta_p)$), a ranking (e.g. $rank(\boldsymbol{\beta}) : \mathbf{r} = (r_1, \ldots, r_m)$) and a subset of features (e.g. $\mathbf{s} = (s_1, \ldots, s_p), s_j = \mathbb{I}\{\beta_j \neq 0\}$ where $\mathbb{I}\{\cdot\}$ is the indicator function). In the CLUST and ECLUST methods, we defined a predictor to be non-zero if its corresponding cluster representative weight was non-zero. Using 10-fold cross validation (CV), we evaluated the similarity between two features and their rankings using Pearson and Spearman correlation, respectively. For each CV fold we re-ran the models and took the average Pearson/Spearman correlations of the $\binom{10}{2}$ combinations of estimated coefficients vectors. To measure the similarity between two subsets of features we took the average of the Jaccard distance in each fold. A Jaccard distance of 1 indicates perfect agreement between two sets while no agreement will result in a distance of 0. For MARS models we do not report the Pearson/Spearman stability rankings due to the adaptive and functional nature of the model (there are many possible combinations of predictors, each of which are linear basis functions).

3.3.4 Results

All reported results are based on 200 simulation runs. We graphically summarized the results across simulations 1-3 for model fit (Figure 3.5) and feature stability (Figure 3.6). The results for simulations 4-6 are shown in the Supplemental Section B, Figures S1-S6. We restrict our attention to $SNR = 1$, $\rho = 0.9$, and $\alpha_j \sim \text{Unif}[1.9, 2.1]$. The model names are labeled as `summary measure_model` (e.g. `avg_lasso` corresponds using the average of the features in a cluster as inputs into a lasso regression model). When there is no summary measure appearing in the model name, that indicates that the original variables were used (e.g. `enet` means all separate features were used in the elasticnet model). In panel A of Figure 3.5, we plot the true positive rate against the false positive rate for each of the

Table 3.3: Measures of Performance

Measure	Formula
Model Fit	
True Positive Rate (TPR)	$|\widehat{S} \in S_0|\big/|S_0|$
False Positive Rate (TPR)	$|\widehat{S} \notin S_0|\big/|j \notin S_0|$
Correct Sparsity (Witten et al., 2014)	$\frac{1}{p}\sum_{j=1}^{p} A_j$
	$A_j = \begin{cases} 1 & \text{if } \hat{\beta}_j = \beta_j = 0 \\ 1 & \text{if } \hat{\beta}_j \neq 0, \beta_j \neq 0 \\ 0 & \text{if else} \end{cases}$
Prediction Accuracy	
Root Mean Squared Error (RMSE)	$\|\mathbf{Y}_{test} - \widehat{\boldsymbol{\mu}}(\mathbf{X}_{test})\|_2$
Area Under the Curve (AUC)	Trapezoidal rule
Hosmer-Lemeshow Test ($G = 10$)	χ^2 test statistic
Feature Stability using K-fold Cross-Validation on training set (Kalousis et al., 2007)	
Pearson Correlation (ρ) (Pearson, 1895)	$\binom{K}{2}^{-1} \sum\limits_{i,j\in\{1,\dots,K\},i\neq j} \frac{cov\left(\widehat{\beta}_{(i)},\widehat{\beta}_{(j)}\right)}{\sigma_{\widehat{\beta}_{(i)}}\sigma_{\widehat{\beta}_{(j)}}}$
Spearman Correlation (r) (Spearman, 1904)	$\binom{K}{2}^{-1} \sum\limits_{i,j\in\{1,\dots,K\},i\neq j} \left[1 - 6\sum\limits_{m} \frac{\left(r_{m_{(i)}}-r_{m_{(j)}}\right)^2}{p(p^2-1)}\right]$
Jaccard Distance (Jaccard, 1912)	$\frac{|\widehat{S}_{(i)}\cap\widehat{S}_{(j)}|}{|\widehat{S}_{(i)}\cup\widehat{S}_{(j)}|}$

[a]$\widehat{\boldsymbol{\mu}}$: fitting procedure on the training set [b]S_0: index of active set $= \left\{j; \beta_j^0 \neq 0\right\}$ [c]$\widehat{S}$: index of the set of non-zero estimated coefficients $= \left\{j; \widehat{\beta}_j \neq 0\right\}$ [d]$|A|$: is the cardinality of set A

200 simulations. We see that across all simulation scenarios, the SEPARATE method has extremely poor sensitivity compared to both CLUST and ECLUST, which do much better at identifying the active variables, though the resulting models are not always sparse. The relatively few number of green points in panel A is due to the small number of estimated clusters (Supplemental Section C, Figure S7) leading to very little variability in performance across simulations. The better performance of ECLUST over CLUST is noticeable as more points lie in the top left part of the plot. The horizontal banding in panel A reflects the stability of the TOM-based clustering approach. ECLUST also does better than CLUST in
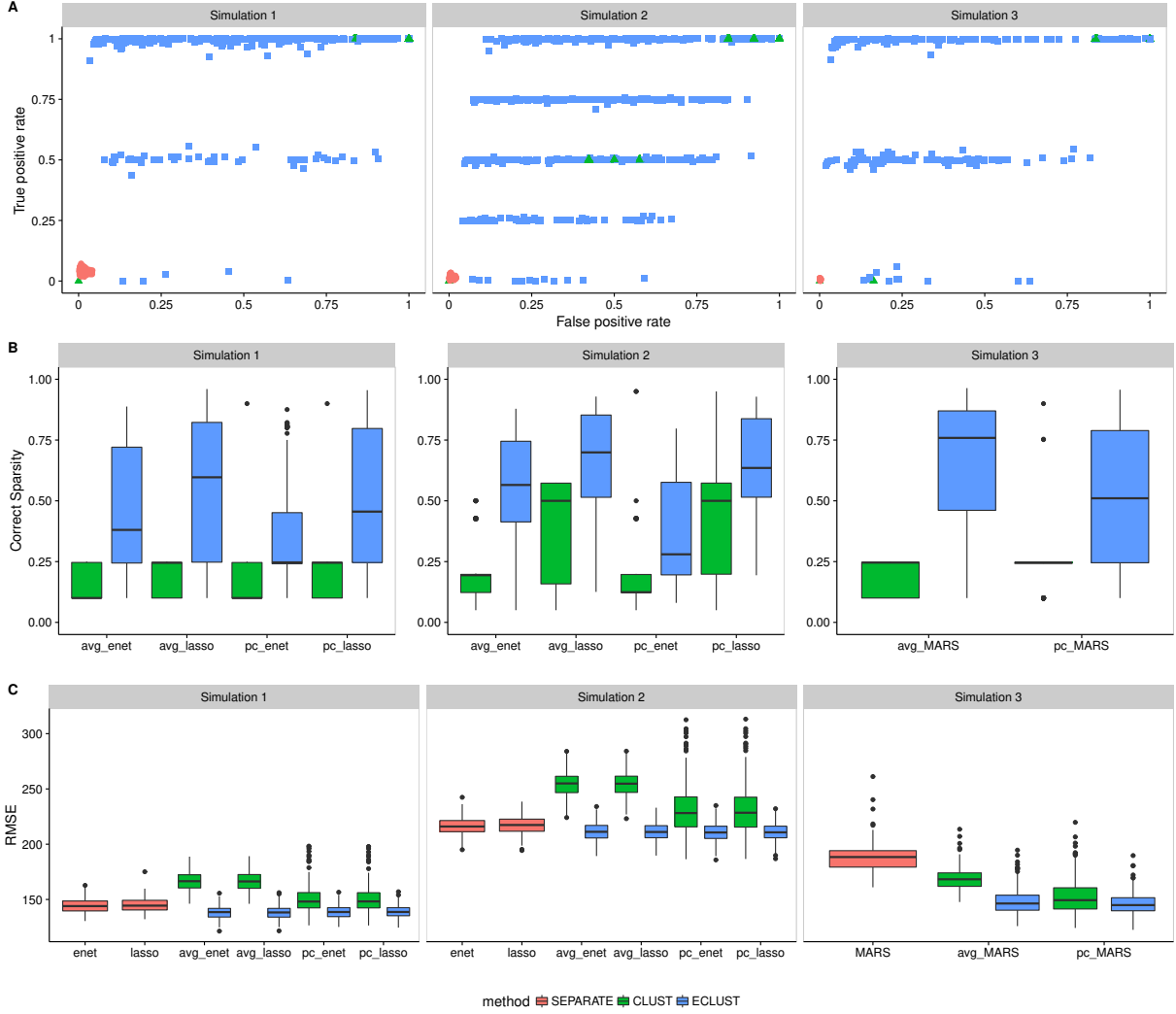
Figure 3.5: Model fit results from simulations 1, 2 and 3 with $SNR = 1$, $\rho = 0.9$, and $\alpha_j \sim \mathrm{Unif}\,[1.9, 2.1]$. SEPARATE results are in pink, CLUST in green and ECLUST in blue.

correctly determining whether a feature is zero or nonzero (Figure 3.5, panel B). Importantly, across all three simulation scenarios, ECLUST outperforms the competing methods in terms of RMSE (Figure 3.5, panel C), regardless of the summary measure and modeling procedure. We present the distribution for the effective number of variables selected in the supplemental material (Figures S8 and S9). We see that the median number of variables selected from ECLUST is less than the median number of variables selected from CLUST, though ECLUST has more variability.

While the approach using all separate original variables (SEPARATE) produce sparse mod-

els, they are sensitive to small perturbations of the data across all stability measures (Figure 3.6), i.e, similar datasets produce very different models. Although the median for the CLUST approach is always slightly better than the median for ECLUST across all stability measures, CLUST results can be much more variable, particularly when stability is measured by the agreement between the value and the ranking of the estimated coefficients across CV folds (Figure 3.6, panels B and C). The number of estimated clusters, and therefore the number of features in the regression model, tends to be much smaller in CLUST compared to ECLUST, and this explains its poorer performance using the stability measures in Figure 3.6, since there are more coefficients to estimate. Overall, we observe that the relative performance of ECLUST versus CLUST in terms of stability is consistent across the two summary measures (average or principal component) and across the penalization procedures. The complete results for different values of ρ, SNR and α_j (when applicable) are available in the Supplemental Section D, Figures S10-S15 for Simulation 1, Figures S16 - S21 for Simulation 2, and Figures S22 - S25 for Simulation 3. They show that these conclusions are not sensitive to the SNR, ρ or α_j. Similar conclusions are made for a binary outcome using logistic regression versions of the lasso, elasticnet and MARS. ECLUST and CLUST also have better calibration than the SEPARATE method for both linear and non-linear models (Supplemental Section B, Figures S3-S6). The distributions of Hosmer-Lemeshow (HL) p-values do not follow uniformity. This is in part due to the fact that the HL test has low power in the presence of continuous-dichotomous variable interactions (Hosmer et al., 1997). Upon inspection of the Q-Q plots, we see that the models have difficulty predicting risks at the boundaries which is a known issue in most models. We also have a small sample size of 200, which means there are on average only 20 subjects in each of the 10 bins. Furthermore, the HL test is sensitive to the choice of bins and method of computing quantiles. Nevertheless, the improved fit relative to the SEPARATE analysis is quite clear.

We also ran all our simulations using the Pearson correlation matrix as a measure of similarity in order to compare its performance against the TOM. The complete results are in the
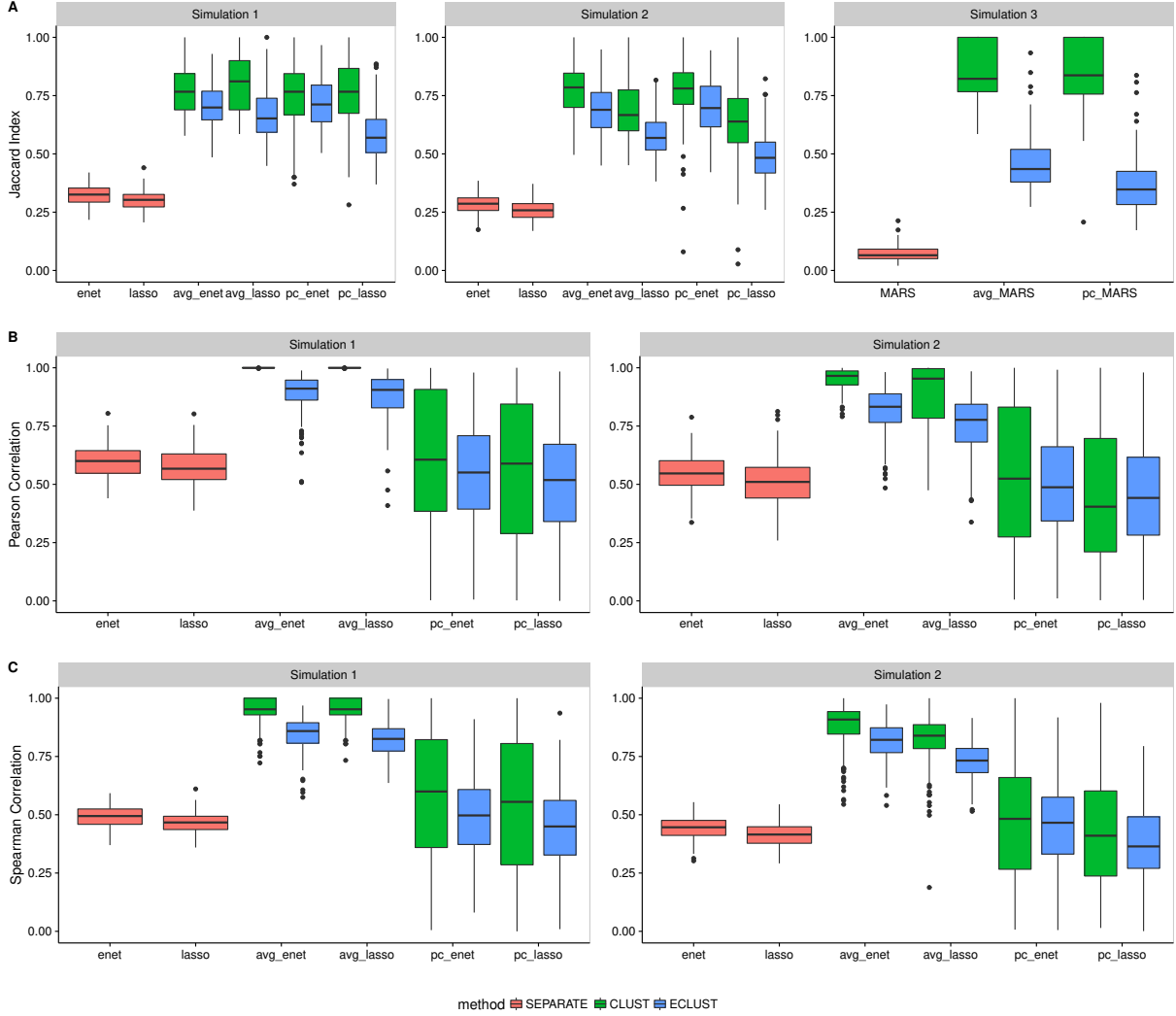
Figure 3.6: Stability results from simulations 1, 2 and 3 for $SNR = 1$, $\rho = 0.9$, and $\alpha_j \sim \mathrm{Unif}[1.9, 2.1]$. SEPARATE results are in pink, CLUST in green and ECLUST in blue.

Supplemental Section E, Figures S26-S31 for Simulation 1, Figures S32 - S37 for Simulation 2, and Figures S38 - S41 for Simulation 3. In general, we see slightly better performance of CLUST over ECLUST when using Pearson correlations. This result is probably due to the imprecision in the estimated correlations. The exposure dependent similarity matrices are quite noisy, and the variability is even larger when we examine the differences between two correlation matrices. Such large levels of variability have a negative impact on the clustering algorithm's ability to detecting the true clusters.

3.4 Analysis of three data sets

In this section we demonstrate the performance of ECLUST on three high dimensional datasets with contrasting motivations and features. In the first data set, normal brain development is examined in conjunction with intelligence scores. In the second data set we aim to identify molecular subtypes of ovarian cancer using gene expression data. The investigators' goal in the third data set is to examine the impact of gestational diabetes mellitus (GDM) on childhood obesity in a sample of mother-child pairs from a prospective birth cohort. The datasets comprise a range of sample sizes, and both the amount of clustering in the HD data and the strength of the effects of the designated exposure variables vary substantially. Due to the complex nature of these datasets, we decided to use MARS models for step 2 of our algorithm for all 3 datasets, as outlined in Table 3.1. In order to assess performance in these data sets, we have computed the 0.632 estimator (Efron, 1983) and the 95% confidence interval of the R^2 and RMSE from 100 bootstrap samples. The R^2 reported here is defined as the squared Pearson correlation coefficient between the observed and predicted response (Kvålseth, 1985), and the RMSE is defined as in Table 3.3. Because MARS models can result in unstable predictors (Kuhn, 2008), we also report the results of bagged MARS from $B = 50$ bootstrap samples, where bagging (Breiman, 1996) refers to averaging the predictions from each of the MARS models fit on the B bootstrap samples.

3.4.1 NIH MRI Study of Normal Brain Development

The NIH MRI Study of Normal Brain Development, started in 2001, was a 7 year longitudinal multi-site project that used magnetic resonance technologies to characterize brain maturation in 433 medically healthy, psychiatrically normal children aged 4.5-18 years (Evans et al., 2006). The goal of this study was to provide researchers with a representative and reliable source of healthy control subject data as a basis for understanding atypical brain development

associated with a variety of developmental, neurological, and neuropsychiatric disorders affecting children and adults. Brain imaging data (e.g. cortical surface thickness, intra-cranial volume), behavioural measures (e.g. IQ scores, psychiatric interviews, behavioral ratings) and demographics (e.g. socioeconomic status) were collected at two year intervals for three time points and are publicly available upon request. Previous research using these data found that level of intelligence and age correlate with cortical thickness (Khundrakpam et al., 2013; Shaw et al., 2006), but to our knowledge no such relation between income and cortical thickness has been observed. We therefore used this data to see the performance of ECLUST in the presence (age) and absence (income) of an effect on the correlations in the HD data. We analyzed the 10,000 most variable regions on the cortical surface from brain scans corresponding to the first sampled time point only. We used binary age (166 age ≤ 11.3 and $172 > 11.3$) and binary income (142 high and 133 low income) indicator as the environment variables and standardized IQ scores as the response. We identified 22 clusters from $TOM(X_{\mathrm{all}})$ and 57 clusters from $TOM(X_{\mathrm{diff}})$ when using age as the environment, and 86 clusters from $TOM(X_{\mathrm{all}})$ and 49 clusters from $TOM(X_{\mathrm{diff}})$ when using income as the environment. Results are shown in Figure 3.7, panels C and D. The method which uses all individual variables as predictors (pink), has better R^2 but also worse RMSE compared to CLUST and ECLUST, likely due to over-fitting. There is a slight benefit in performance for ECLUST over CLUST when using age as the environment (panel D). Importantly, we observe very similar performance between CLUST and ECLUST across all models (panel C), suggesting very little impact on the prediction performance when including features derived both with and without the E variable, in a situation where they are unlikely to be relevant.

3.4.2 Gene Expression Study of Ovarian Cancer

Differences in gene expression profiles have led to the identification of robust molecular subtypes of ovarian cancer; these are of biological and clinical importance because they have been shown to correlate with overall survival (Tothill et al., 2008). Improving prediction of survival time based on gene expression signatures can lead to targeted therapeutic interventions (Helland et al., 2011). The proposed ECLUST algorithm was applied to gene expression data from 511 ovarian cancer patients profiled by the Affymetrix Human Genome U133A 2.0 Array. The data were obtained from the TCGA Research Network: http://cancergenome.nih.gov/ and downloaded via the TCGA2STAT R library (Wan et al., 2015). Using the 881 signature genes from Helland et al. (2011) we grouped subjects into two groups based on the results in this paper, to create a "positive control" environmental variable expected to have a strong effect. Specifically, we defined an environment variable in our framework as: $E = 0$ for subtypes C1 and C2 ($n = 253$), and $E = 1$ for subtypes C4 and C5 ($n = 258$). Overall survival time (log transformed) was used as the response variable. Since these genes were ascertained on survival time, we expected the method using all genes without clustering to have the best performance, and hence one goal of this analysis was to see if ECLUST performed significantly worse as a result of summarizing the data into a lower dimension. We found 3 clusters from $TOM(X_{\mathrm{all}})$ and 3 clusters from $TOM(X_{\mathrm{diff}})$; results are shown in Figure 3.7, panel C. Across all models, ECLUST performs slightly better than CLUST. Furthermore it performs almost as well as the separate variable method, with the added advantage of dealing with a much smaller number of predictors (881 with SEPARATE compared to 6 with ECLUST).

3.4.3 Gestational diabetes, epigenetics and metabolic disease

Events during pregnancy are suspected to play a role in childhood obesity development but only little is known about the mechanisms involved. Indeed, children born to women who

had GDM in pregnancy are more likely to be overweight and obese (Wendland et al., 2012), and evidence suggests epigenetic factors are important piece of the puzzle (Bouchard et al., 2012, 2010). Recently, methylation changes in placenta and cord blood were associated with GDM (Ruchat et al., 2013), and here we explore how these changes are associated with obesity in the children at the age of about 5 years old. DNA methylation in placenta was measured with the Infinium HumanMethylation450 BeadChip (Illumina, Inc (Bibikova et al., 2011)) microarray, in a sample of 28 women, 20 of whom had a GDM-affected pregnancy, and here, we used GDM status as our E variable, assuming that this has widespread effects on DNA methylation and on its correlation patterns. Our response, Y, is the standardized body mass index (BMI) in the offspring at the age of 5. In contrast to the previous two examples, here we had no particular expectation of how ECLUST would perform. Using the 10,000 most variable probes, we found 2 clusters from $TOM(X_{\text{all}})$, and 75 clusters from $TOM(X_{\text{diff}})$. The predictive model results from a MARS analysis are shown in Figure 3.7, panel A. When using R^2 as the measure of performance, ECLUST outperforms both SEPARATE and CLUST methods. When using RMSE as the measure of model performance, performance tended to be better with CLUST rather than ECLUST perhaps in part due to the small number of clusters derived from $TOM(X_{\text{all}})$ relative to $TOM(X_{\text{diff}})$. Overall, the ECLUST algorithm with bagged MARS and the 1st PC of each cluster performed best, i.e., it had a better R^2 than CLUST with comparable RMSE. The sample size here is very small, and therefore the stability of the model fits is limited stability.

The probes in these clusters mapped to 164 genes and these genes were selected to conduct pathway analyses using the Ingenuity Pathway Analysis (IPA) software (Ingenuity System). IPA compares the selected genes to a reference list of genes included in many biological pathways using a hypergeometric test. Smaller p values are evidence for over-represented gene ontology categories in the input gene list. The results are summarized in Table 3.4 and provide some biological validation of our ECLUST method. For example, the Hepatic system is involved with the metabolism of glucose and lipids (Saltiel & Kahn, 2001), and behavior
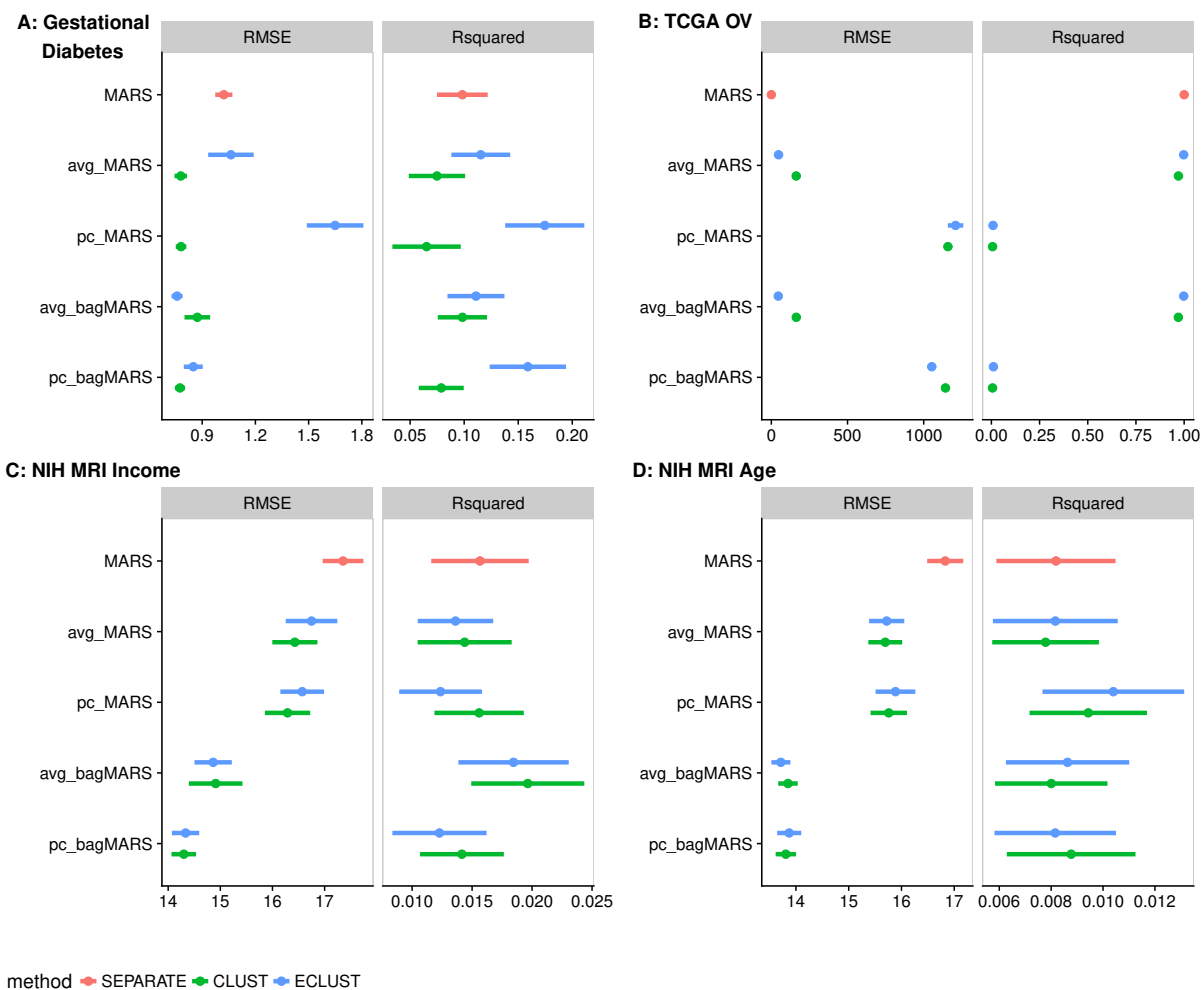
Figure 3.7: Model fit measures from analysis of three data sets: (A) Gestational diabetes birth-cohort (B) TCGA Ovarian Cancer study (C) NIH MRI Study with income as the environment variable (D) NIH MRI Study with age as the environment variable.

and neurodevelopment are associated with obesity (Epstein et al., 2004). Furthermore, it is interesting that embryonic and organ development pathways are involved since GDM is associated with macrosomia (Ehrenberg et al., 2004).

Table 3.4: Ingenuity Pathway Analysis Results – top-ranked diseases and disorders, and physiological system development and function epigentically affected by gestational diabetes mellitus and associated with childhood body mass index

Category	Name	p values	n^a
Diseases and Disorders	Hepatic System Disease	[9.61e−7 − 5.17e−7]	75
Physiological System Development and Function			
	Behavior	[1.35e−2 − 7.82e−8]	33
	Embryonic Development	[1.35e−2 − 2.63e−8]	26
	Nervous System Development and Function	[1.35e−2 − 2.63e−8]	43
	Organ Development	[1.35e−2 − 2.63e−8]	20
	Organismal Development	[1.35e−2 − 2.63e−8]	34

[a]number of genes involved in each pathway

3.5 Discussion

The challenge of precision medicine is to appropriately fit treatments or recommendations to each individual. Data such as gene expression, DNA methylation levels, or magnetic resonance imaging (MRI) signals are examples of HD measurements that capture multiple aspects of how a tissue is functioning. These data often show patterns associated with disease, and major investments are being made in the genomics research community to generate such HD data. Analytic tools increasing prediction accuracy are needed to maximize the productivity of these investments. However, the effects of exposures have usually been overlooked, but these are crucial since they can lead to ways to intervene. Hence, it is essential to have a clear understanding of how exposures modify HD measures, and how the combination leads to disease. Existing methods for prediction (of disease), that are based on HD data and interactions with exposures, fall far short of being able to obtain

this clear understanding. Most methods have low power and poor interpretability, and furthermore, modelling and interpretation problems are exacerbated when there is interest in interactions. In general, power to estimate interactions is low, and the number of possible interactions could be enormous. Therefore, here we have proposed a strategy to leverage situations where a covariate (e.g. an exposure) has a wide-spread effect on one or more HD measures, e.g. GDM on methylation levels. We have shown that this expected pattern can be used to construct dimension-reduced predictor variables that inherently capture the systemic covariate effects. These dimension-reduced variables, constructed without using the phenotype, can then be used in predictive models of any type. In contrast to some common analysis strategies that model the effects of individual predictors on outcome, our approach makes a step towards a systems-based perspective that we believe will be more informative when exploring the factors that are associated with disease or a phenotype of interest. We have shown, through simulations and real data analysis, that incorporation of environmental factors into predictive models in a way that retains a high dimensional perspective can improve results and interpretation for both linear and non linear effects.

We proposed two key methodological steps necessary to maximize predictive model interpretability when using HD data and a binary exposure: (1) dimension reduction of HD data built on exposure sensitivity, and (2) implementation of penalized prediction models. In the first step, we proposed to identify exposure-sensitive HD pairs by contrasting the TOM between exposed and unexposed individuals; then we cluster the elements in these HD pairs to find exposure-sensitive co-regulated sets. New dimension-reduced variables that capture exposure-sensitive features (e.g. the first principal component of each cluster) were then defined. In the second step we implemented linear and non-linear variable selection methods using the dimension-reduced variables to ensure stability of the predictive model. The ECLUST method has been implemented in the `eclust` (Bhatnagar, 2017) R package publicly available on CRAN. Our method along with computationally efficient algorithms, allows for the analysis of up to 10,000 variables at a time on a laptop computer.

The methods that we have proposed here are currently only applicable when three data elements are available. Specifically a binary environmental exposure, a high dimensional dataset that can be affected by the exposure, and a single phenotype. When comparing the TOM and Pearson correlations as a measure of similarity, our simulations showed that the performance of ECLUST was worse with correlations. This speaks to the potential of developing a better measure than the difference of two matrices. For example, we are currently exploring ways in which to handle continuous exposures or multiple exposures. The best way to construct an exposure-sensitive distance matrix that can be used for clustering is not obvious in these situations. One possible solution relies on a non-parametric smoothing based approach where weighted correlations are calculated. These weights can be derived from a kernel-based summary of the exposure covariates (e.g. (Qiu et al., 2016)). Then, contrasting unweighted and weighted matrices will allow construction of covariate-sensitive clusters. The choice of summary measure for each cluster also warrants further study. While principal components and averages are well understood and easy to implement, the main shortcoming is that they involve all original variables in the group. As the size of the groups increase, the interpretability of these measures decreases. Non-negative matrix factorization (Lee & Seung, 2001) and sparse principal component analysis (SPCA) (Witten et al., 2009) are alternatives which find sparse and potentially interpretable factors. Furthermore, structured SPCA (Jenatton et al., 2009) goes beyond restricting the cardinality of the contributing factors by imposing some a priori structural constraints deemed relevant to model the data at hand.

We are all aware that our exposures and environments impact our health and risks of disease, however detecting how the environment acts is extremely difficult. Furthermore, it is very challenging to develop reliable and understandable ways of predicting the risk of disease in individuals, based on high dimensional data such as genomic or imaging measures, and this challenge is exacerbated when there are environmental exposures that lead to many subtle alterations in the genomic measurements. Hence, we have developed an algorithm

and an easy-to use software package to transform analysis of how environmental exposures impact human health, through an innovative signal-extracting approach for high dimensional measurements. Evidently, the model fitting here is performed using existing methods; our goal is to illustrate the potential of improved dimension reduction in two-stage methods, in order to generate discussion and new perspectives. If such an approach can lead to more interpretable results that identify gene-environment interactions and their effects on diseases and traits, the resulting understanding of how exposures influence the high-volume measurements now available in precision medicine will have important implications for health management and drug discovery.

Availability of data and material

1. NIH MRI Study of Normal Brain Development data are available in the Pediatric MRI Data Repository, https://pediatricmri.nih.gov/

2. Gene Expression Study of Ovarian Cancer data are available in the Genomic Data Commons repository, https://gdc.cancer.gov/, and were downloaded via the TCGA2STAT R library (Wan et al., 2015)

3. Gestational diabetes, epigenetics and metabolic disease: the clinical data, similarity matrices and cluster summaries are available at Zenodo [10.5281/zenodo.259222]. The raw analysed during the current study are not publicly available due to reasons of confidentiality, although specific collaborations with LB can be requested.

Competing interests

The authors declare that they have no competing interests.

Author's contributions

SRB, CMTG, YY, MB: conceptualization; SRB, LB, BK: data curation; SRB: formal analysis, software, visualization; SRB, CMTG: methodology; SRB, CMTG: writing-original draft; SRB, CMTG, YY, BK, ACE, MB, LB: writing-review & editing.

Acknowledgements

Additional Files

Additional file 1 – Supplemental Methods and Simulation Results

Contains the following sections:

A **Description of Topological Overlap Matrix** - detailed description of the TOM

B **Binary Outcome Simulation Results** - results of simulations 4, 5 and 6

C **Analysis of Clusters** - number of estimated clusters by different measures of similarity

D **Simulation Results Using TOM as a Measure of Similarity** - detailed simulation results using TOM as a measure of similarity

E **Simulation Results Using Pearson Correlations as a Measure of Similarity** - detailed simulation results using Pearson Correlations as a measure of similarity

F **Visual Representation of Similarity Matrices** - similarity matrices based on Pearson's correlation coefficient

References

Bach, F., Jenatton, R., Mairal, J., Obozinski, G., et al. (2012). Structured sparsity through convex optimization. *Statistical Science*, *27*(4), 450–468.

8

Bertsekas, D. P. (1999). *Nonlinear programming*. Athena scientific Belmont.

13

Bhatnagar, S. R. (2017). eclust: Environment based clustering for interpretable predictive models in high dimensional data [Computer software manual]. Retrieved from https://cran.r-project.org/package=eclust (R package version 0.1.0)

37, 61

Bhatnagar, S. R., Yang, Y., Khundrakpam, B., Evans, A. C., Blanchette, M., Bouchard, L., & Greenwood, C. M. (2018). An analytic approach for interpretable predictive models in high-dimensional data in the presence of interactions with exposures. *Genetic epidemiology*, *42*(3), 233–249.

9

Bibikova, M., Barnes, B., Tsan, C., Ho, V., Klotzle, B., Le, J. M., . . . others (2011). High density dna methylation array with single cpg site resolution. *Genomics*, *98*(4), 288–295.

58

Bien, J., Taylor, J., Tibshirani, R., et al. (2013). A lasso for hierarchical interactions. *The Annals of Statistics*, *41*(3), 1111–1141.

27, 28

Bouchard, L., Hivert, M.-F., Guay, S.-P., St-Pierre, J., Perron, P., & Brisson, D. (2012). Placental adiponectin gene dna methylation levels are associated with mothers' blood glucose concentration. *Diabetes*, *61*(5), 1272–1280.

58

Bouchard, L., Thibault, S., Guay, S.-P., Santure, M., Monpetit, A., St-Pierre, J., . . . Brisson, D. (2010). Leptin gene epigenetic adaptation to impaired glucose metabolism during pregnancy. *Diabetes care*, *33*(11), 2436–2441.

58

Breiman, L. (1996). Bagging predictors. *Machine learning*, *24*(2), 123–140.

55

Bühlmann, P., Rütimann, P., van de Geer, S., & Zhang, C.-H. (2013). Correlated variables in regression: clustering and sparse estimation. *Journal of Statistical Planning and Inference*, *143*(11), 1835–1858.

7, 8, 34, 41

Bühlmann, P., & Van De Geer, S. (2011). *Statistics for high-dimensional data: methods, theory and applications*. Springer Science & Business Media.

10, 19

Chipman, H. (1996). Bayesian variable selection with related predictors. *Canadian Journal of Statistics*, *24*(1), 17–36.

27

Choi, N. H., Li, W., & Zhu, J. (2010). Variable selection with the strong heredity constraint

and its oracle property. *Journal of the American Statistical Association*, *105*(489), 354–364.

28

Cox, D. R. (1984). Interaction. *International Statistical Review/Revue Internationale de Statistique*, 1–24.

26

Efron, B. (1983). Estimating the error rate of a prediction rule: improvement on cross-validation. *Journal of the American Statistical Association*, *78*(382), 316–331.

55

Efron, B., Hastie, T., Johnstone, I., Tibshirani, R., et al. (2004). Least angle regression. *The Annals of statistics*, *32*(2), 407–499.

10

Ehrenberg, H. M., Mercer, B. M., & Catalano, P. M. (2004). The influence of obesity and diabetes on the prevalence of macrosomia. *American journal of obstetrics and gynecology*, *191*(3), 964–968.

60

Epstein, L. H., Paluch, R. A., Kilanowski, C. K., & Raynor, H. A. (2004). The effect of reinforcement or stimulus control to reduce sedentary behavior in the treatment of pediatric obesity. *Health Psychology*, *23*(4), 371.

60

Evans, A. C., Group, B. D. C., et al. (2006). The nih mri study of normal brain development. *Neuroimage*, *30*(1), 184–202.

55

Fan, J., Han, F., & Liu, H. (2014). Challenges of big data analysis. *National science review*, *1*(2), 293–314.

2, 33

Fan, J., & Li, R. (2001). Variable selection via nonconcave penalized likelihood and its oracle properties. *Journal of the American statistical Association*, *96*(456), 1348–1360.

7, 19

Felson, D. T., Zhang, Y., Hannan, M. T., & Anderson, J. J. (1993). Effects of weight and body mass index on bone mineral density in men and women: the framingham study. *Journal of Bone and Mineral Research*, *8*(5), 567–573.

49

Friedman, J., Hastie, T., Höfling, H., Tibshirani, R., et al. (2007). Pathwise coordinate optimization. *The Annals of Applied Statistics*, *1*(2), 302–332.

10

Friedman, J., Hastie, T., & Tibshirani, R. (2001). *The elements of statistical learning* (Vol. 1). Springer series in statistics Springer, Berlin.

2

Friedman, J., Hastie, T., & Tibshirani, R. (2010). Regularization paths for generalized linear models via coordinate descent. *Journal of statistical software*, *33*(1), 1.

9, 11, 18, 33, 43

Friedman, J. H. (1991). Multivariate adaptive regression splines. *The annals of statistics*, 1–67.

41, 45

Gibson, G. (2009). Decanalization and the origin of complex disease. *Nature reviews. Genetics*, *10*(2), 134.

48

Hao, N., Feng, Y., & Zhang, H. H. (2018). Model selection for high-dimensional quadratic regression via regularization. *Journal of the American Statistical Association*, 1–11.
28

Haris, A., Witten, D., & Simon, N. (2014). Convex modeling of interactions with strong heredity. *arXiv preprint arXiv:1410.3517*.
27

Haris, A., Witten, D., & Simon, N. (2016). Convex modeling of interactions with strong heredity. *Journal of Computational and Graphical Statistics*, *25*(4), 981–1004.
28

Hastie, T., Tibshirani, R., Botstein, D., & Brown, P. (2001). Supervised harvesting of expression trees. *Genome Biology*, *2*(1), 1–0003.
8, 33

Helland, Å., Anglesio, M. S., George, J., Cowin, P. A., Johnstone, C. N., House, C. M., . . . others (2011). Deregulation of mycn, lin28b and let7 in a molecular subtype of aggressive high-grade serous ovarian cancers. *PloS one*, *6*(4), e18064.
57

Hoerl, A. E., & Kennard, R. W. (1970). Ridge regression: Biased estimation for nonorthogonal problems. *Technometrics*, *12*(1), 55–67.
7

Hosmer, D. W., Hosmer, T., Le Cessie, S., Lemeshow, S., et al. (1997). A comparison of goodness-of-fit tests for the logistic regression model. *Statistics in medicine*, *16*(9), 965–980.
53

Jaccard, P. (1912). The distribution of the flora in the alpine zone. *New phytologist*, *11*(2), 37–50.

51

Jacob, L., Obozinski, G., & Vert, J.-P. (2009). Group lasso with overlap and graph lasso. In *Proceedings of the 26th annual international conference on machine learning* (pp. 433–440).

28

Jenatton, R., Obozinski, G., & Bach, F. (2009). Structured sparse principal component analysis. *arXiv preprint arXiv:0909.1440*.

62

Kalousis, A., Prados, J., & Hilario, M. (2007). Stability of feature selection algorithms: a study on high-dimensional spaces. *Knowledge and information systems*, *12*(1), 95–116.

51

Kanehisa, M., Araki, M., Goto, S., Hattori, M., Hirakawa, M., Itoh, M., . . . others (2008). Kegg for linking genomes to life and the environment. *Nucleic acids research*, *36*(suppl 1), D480–D484.

8

Kemp, J. P., Morris, J. A., Medina-Gomez, C., Forgetta, V., Warrington, N. M., Youlten, S. E., . . . others (2017). Identification of 153 new loci associated with heel bone mineral density and functional involvement of gpc6 in osteoporosis. *Nature genetics*, *49*, 1468.

49

Kendall, M. (1957). *A course in multivariate analysis*. London: Griffin.

8, 33

Khundrakpam, B. S., Reid, A., Brauer, J., Carbonell, F., Lewis, J., Ameis, S., . . . others (2013). Developmental changes in organization of structural brain networks. *Cerebral Cortex*, *23*(9), 2072–2085.

36, 56

Klein, K. O., Oualkacha, K., Lafond, M.-H., Bhatnagar, S., Tonin, P. N., & Greenwood, C. M. (2016). Gene coexpression analyses differentiate networks associated with diverse cancers harboring tp53 missense or null mutations. *Frontiers in Genetics*, *7*.

36, 40

Kostka, D., & Spang, R. (2004). Finding disease specific alterations in the co-expression of genes. *Bioinformatics*, *20*(suppl 1), i194–i199.

36

Kuhn, M. (2008). Caret package. *Journal of Statistical Software*, *28*(5).

33, 55

Kvålseth, T. O. (1985). Cautionary note about r 2. *The American Statistician*, *39*(4), 279–285.

55

Laird, N. M., & Ware, J. H. (1982). Random-effects models for longitudinal data. *Biometrics*, 963–974.

28

Lange, K., Hunter, D., & Yang, I. (2000). Optimization transfer using sur- rogate objective functions (with discussion). *Journal of Computational and Graphical Statistics*, *9*, 1-20.

21

Langfelder, P., & Horvath, S. (2007). Eigengene networks for studying the relationships between co-expression modules. *BMC systems biology*, *1*(1), 54.

41

Langfelder, P., & Horvath, S. (2008). Wgcna: an r package for weighted correlation network analysis. *BMC bioinformatics*, *9*(1), 1.

43

Langfelder, P., Zhang, B., & Horvath, S. (2008). Defining clusters from a hierarchical cluster tree: the dynamic tree cut package for r. *Bioinformatics*, *24*(5), 719–720.
41, 43

Langfelder, P., Zhang, B., & with contributions from Steve Horvath. (2016). dynamictreecut: Methods for detection of clusters in hierarchical clustering dendrograms [Computer software manual]. Retrieved from https://CRAN.R-project.org/package=dynamicTreeCut (R package version 1.63-1)
43

Lee, D. D., & Seung, H. S. (2001). Algorithms for non-negative matrix factorization. In *Advances in neural information processing systems* (pp. 556–562).
62

Leek, J. T., & Storey, J. D. (2008). A general framework for multiple testing dependence. *Proceedings of the National Academy of Sciences*, *105*(48), 18718–18723.
6

Lim, M., & Hastie, T. (2015). Learning interactions via hierarchical group-lasso regularization. *Journal of Computational and Graphical Statistics*, *24*(3), 627–654.
27, 28

Lin, X., Lee, S., Christiani, D. C., & Lin, X. (2013). Test for interactions between a genetic marker set and environment in generalized linear models. *Biostatistics*, kxt006.
6

Manolio, T. A., Collins, F. S., Cox, N. J., Goldstein, D. B., Hindorff, L. A., Hunter, D. J., . . . others (2009). Finding the missing heritability of complex diseases. *Nature*, *461*(7265), 747–753.
6

Meier, L., Van De Geer, S., & Bühlmann, P. (2008). The group lasso for logistic regression. *Journal of the Royal Statistical Society: Series B (Statistical Methodology)*, *70*(1), 53–71.
11

Meinshausen, N. (2007). Relaxed lasso. *Computational Statistics & Data Analysis*, *52*(1), 374–393.
7

Milborrow. Derived from mda:mars by T. Hastie and R. Tibshirani., S. (2011). earth: Multivariate adaptive regression splines [Computer software manual]. Retrieved from http://CRAN.R-project.org/package=earth (R package)
43

Müllner, D. (2013). fastcluster: Fast hierarchical, agglomerative clustering routines for R and Python. *Journal of Statistical Software*, *53*(9), 1–18. Retrieved from http://www.jstatsoft.org/v53/i09/
9, 33

Osborne, M. R., Presnell, B., & Turlach, B. A. (2000). A new approach to variable selection in least squares problems. *IMA journal of numerical analysis*, *20*(3), 389–403.
10

Park, M. Y., Hastie, T., & Tibshirani, R. (2007). Averaged gene expressions for regression. *Biostatistics*, *8*(2), 212–227.
8, 33, 41

Pearson, K. (1895). Note on regression and inheritance in the case of two parents. *Proceedings of the Royal Society of London*, 240–242.
51

Qiu, H., Han, F., Liu, H., & Caffo, B. (2016). Joint estimation of multiple graphical models

from high dimensional time series. *Journal of the Royal Statistical Society: Series B (Statistical Methodology)*, *78*(2), 487–504.

62

R Core Team. (2016). R: A language and environment for statistical computing [Computer software manual]. Vienna, Austria. Retrieved from https://www.R-project.org/

43

Radchenko, P., & James, G. M. (2010). Variable selection using adaptive nonlinear interaction structures in high dimensions. *Journal of the American Statistical Association*, *105*(492), 1541–1553.

27, 28

Ravasz, E., Somera, A. L., Mongru, D. A., Oltvai, Z. N., & Barabási, A.-L. (2002). Hierarchical organization of modularity in metabolic networks. *science*, *297*(5586), 1551–1555.

40

Reid, S., & Tibshirani, R. (2016). Sparse regression and marginal testing using cluster prototypes. *Biostatistics*, *17*(2), 364–376.

34

Reid, S., Tibshirani, R., & Friedman, J. (2016). A study of error variance estimation in lasso regression. *Statistica Sinica*, 35–67.

2

Robin, X., Turck, N., Hainard, A., Tiberti, N., Lisacek, F., Sanchez, J.-C., & Müller, M. (2011). proc: an open-source package for r and s+ to analyze and compare roc curves. *BMC Bioinformatics*, *12*, 77.

49

Ruchat, S.-M., Houde, A.-A., Voisin, G., St-Pierre, J., Perron, P., Baillargeon, J.-P., . . .

Bouchard, L. (2013). Gestational diabetes mellitus epigenetically affects genes predominantly involved in metabolic diseases. *Epigenetics*, *8*(9), 935–943.

58

Saltiel, A. R., & Kahn, C. R. (2001). Insulin signalling and the regulation of glucose and lipid metabolism. *Nature*, *414*(6865), 799–806.

58

Sathirapongsasuti, J. F. (2013). Copdsexualdimorphism.data: Data to support sexually dimorphic and copd differential analysis for gene expression and methylation. [Computer software manual]. (R package version 1.4.0)

34, 35

Sato, J. R., Hoexter, M. Q., de Magalhães Oliveira, P. P., Brammer, M. J., Murphy, D., Ecker, C., . . . others (2013). Inter-regional cortical thickness correlations are associated with autistic symptoms: a machine-learning approach. *Journal of psychiatric research*, *47*(4), 453–459.

40

Schadt, E. E. (2009). Molecular networks as sensors and drivers of common human diseases. *Nature*, *461*(7261), 218–223.

6

Schelldorfer, J., Bühlmann, P., DE, G., & VAN, S. (2011). Estimation for high-dimensional linear mixed-effects models using l1-penalization. *Scandinavian Journal of Statistics*, *38*(2), 197–214.

11

Shah, R. D. (2016). Modelling interactions in high-dimensional data with backtracking. *Journal of Machine Learning Research*, *17*(207), 1–31.

28

Shaw, P., Greenstein, D., Lerch, J., Clasen, L., Lenroot, R., Gogtay, N. e. a., . . . Giedd, J. (2006). Intellectual ability and cortical development in children and adolescents. *Nature*, *440*(7084), 676–679.

56

She, Y., & Jiang, H. (2014). Group regularized estimation under structural hierarchy. *arXiv preprint arXiv:1411.4691*.

27, 28

Spearman, C. (1904). The proof and measurement of association between two things. *The American journal of psychology*, *15*(1), 72–101.

51

Tibshirani, R. (1996). Regression shrinkage and selection via the lasso. *Journal of the Royal Statistical Society. Series B (Methodological)*, 267–288.

7, 10, 41, 45

Tibshirani, R., Saunders, M., Rosset, S., Zhu, J., & Knight, K. (2005). Sparsity and smoothness via the fused lasso. *Journal of the Royal Statistical Society: Series B (Statistical Methodology)*, *67*(1), 91–108.

7

Toloşi, L., & Lengauer, T. (2011). Classification with correlated features: unreliability of feature ranking and solutions. *Bioinformatics*, *27*(14), 1986–1994.

50

Tothill, R. W., Tinker, A. V., George, J., Brown, R., Fox, S. B., Lade, S., . . . others (2008). Novel molecular subtypes of serous and endometrioid ovarian cancer linked to clinical outcome. *Clinical Cancer Research*, *14*(16), 5198–5208.

57

Tseng, P. (2001). Convergence of a block coordinate descent method for nondifferentiable minimization. *Journal of optimization theory and applications*, *109*(3), 475–494. 11

Tseng, P., et al. (1988). Coordinate ascent for maximizing nondifferentiable concave functions. 11

Tseng, P., & Yun, S. (2009). A coordinate gradient descent method for nonsmooth separable minimization. *Mathematical Programming*, *117*(1), 387–423. 10, 11, 13

Tzourio-Mazoyer, N., Landeau, B., Papathanassiou, D., Crivello, F., Etard, O., Delcroix, N., ... Joliot, M. (2002). Automated anatomical labeling of activations in spm using a macroscopic anatomical parcellation of the mni mri single-subject brain. *Neuroimage*, *15*(1), 273–289. 8

Wan, Y.-W., Allen, G. I., Anderson, M. L., & Liu, Z. (2015). Tcga2stat: Simple tcga data access for integrated statistical analysis in r [Computer software manual]. Retrieved from https://CRAN.R-project.org/package=TCGA2STAT (R package version 1.2) 57, 63

Wendland, E. M., Torloni, M. R., Falavigna, M., Trujillo, J., Dode, M. A., Campos, M. A., ... Schmidt, M. I. (2012). Gestational diabetes and pregnancy outcomes-a systematic review of the world health organization (who) and the international association of diabetes in pregnancy study groups (iadpsg) diagnostic criteria. *BMC pregnancy and childbirth*, *12*(1), 1. 58

Witten, D. M., Shojaie, A., & Zhang, F. (2014). The cluster elastic net for high-dimensional regression with unknown variable grouping. *Technometrics*, *56*(1), 112–122.

9, 51

Witten, D. M., Tibshirani, R., & Hastie, T. (2009). A penalized matrix decomposition, with applications to sparse principal components and canonical correlation analysis. *Biostatistics*, kxp008.

62

Yang, J., Benyamin, B., McEvoy, B. P., Gordon, S., Henders, A. K., Nyholt, D. R., ... others (2010). Common snps explain a large proportion of the heritability for human height. *Nature genetics*, *42*(7), 565.

6

Yang, Y., & Zou, H. (2014). gglasso: Group lasso penalized learning using a unified bmd algorithm. Retrieved from http://CRAN.R-project.org/package=gglasso (R package version 1.3)

9, 33

Yang, Y., & Zou, H. (2015). A fast unified algorithm for solving group-lasso penalize learning problems. *Statistics and Computing*, *25*(6), 1129–1141.

21, 22, 23

Yuan, M., & Lin, Y. (2006). Model selection and estimation in regression with grouped variables. *Journal of the Royal Statistical Society: Series B (Statistical Methodology)*, *68*(1), 49–67.

8, 21

Zhang, B., & Horvath, S. (2005). A general framework for weighted gene co-expression network analysis. *Statistical applications in genetics and molecular biology*, *4*(1).

40

Zhang, C.-H. (2010). Nearly unbiased variable selection under minimax concave penalty. *The Annals of Statistics*, 894–942.

7

Zhao, P., Rocha, G., & Yu, B. (2009). The composite absolute penalties family for grouped and hierarchical variable selection. *The Annals of Statistics*, 3468–3497.

27, 28

Zou, H. (2006). The adaptive lasso and its oracle properties. *Journal of the American statistical association*, *101*(476), 1418–1429.

7, 10, 19

Zou, H., & Hastie, T. (2005). Regularization and variable selection via the elastic net. *Journal of the Royal Statistical Society: Series B (Statistical Methodology)*, *67*(2), 301–320.

7, 41, 45